DEPARTMENT OF MATERIALS SCIENCE

NOVA SCHOOL OF SCIENCE & TECHNOLOGY

CAROLINA DO ROSÁRIO MARTINS BELLO

BSc in Micro and Nanotechnologies Engineering

DEVELOPMENT OF MAGNETIC CLAYS WITH CATALYTIC ACTIVITY FOR CANCER TREATMENT APPLICATION

MASTER IN MICRO AND NANOTECHNOLOGIES ENGINEERING

NOVA University Lisbon
March of 2023

DEPARTMENT OF MATERIALS SCIENCE

Development of magnetic clays with catalytic activity for cancer treatment application

Carolina do Rosário Martins Bello

BSc in Micro and Nanotechnologies Engineering

Adviser: Dr. Paula I. P. Soares
Principal Researcher, *NOVA University Lisbon*

Co-advisers: Dr. Susana Barreiros
Professor, *NOVA University Lisbon*

Examination Committee:

Chair: Dr. Maria Helena Figueiredo Godinho,
Associate Professor, NOVA University Lisbon

Rapporteurs: Dr. Alexandre Babo de Almeida Paiva,
Associate Professor, NOVA University Lisbon

Adviser: Dr. Paula I.P Soares
Principal Researcher, NOVA University Lisbon

Master in Micro and Nanotechnologies Engineering

NOVA University Lisbon
March of 2023

“It always seems impossible until it's done.”

ACKNOWLEDGMENTS

Em primeiro lugar, gostaria de agradecer à minha orientadora, Prof. Dra. Paula Soares pela confiança depositada em mim na escolha deste tema, e por me ter recebido no laboratório 107 dando-me a oportunidade de o desenvolver. Agradeço também com enorme carinho à minha coorientadora Prof. Dra. Susana Barreiros todo o apoio, disponibilidade e palavras de incentivo que nunca me fizeram desistir, mesmo quando tudo parecia estar errado. Ambas foram cruciais neste processo e muito atenciosas comigo, tornando tudo mais fácil e motivante.

Obrigada a toda a equipa do laboratório 107 do DCM, com especial atenção à amorosa Augusta, que esteve sempre pronta a cuidar de nós, como se de uns filhos nos tratássemos. Nunca vou esquecer quando deixei cair frascos e parti duas provetas e a preocupação foi, só e apenas, saber se me tinha cortado. Uma querida!

Ao laboratório 427 no DQ, grata pelo auxílio que me prestaram sempre que necessário acolhendo esta “intrusa” no vosso “cantinho de química”.

Ao grande Cezar e à querida Adriana um agradecimento especial por terem tomado o papel quase de orientadores estando constantemente ao meu lado para me ensinar com a maior das paciências. O vosso apoio foi mesmo muito essencial.

Aos meus colegas do Lab 107, Leonor, André, Francisco, um enorme obrigada pela entreajuda e momentos de convívio que muito facilitaram todo este processo. Um especial à Leonor que teve a coragem de meter conversa comigo, e que se tornou uma amiga para a vida! Obrigada por todos os conselhos, pelas conversas entre "sínteses" e por me levares umas "bolachinhas calóricas" a meio da tarde quando sabias que não tinha tido tempo para almoçar. És muito importante.

Ao André, um obrigada especial, também, pelas vezes que me acompanhou ao U.V, arranjando-me o cartão sempre que precisava.

Agradeço também ao curso e à vida pelos amigos que me deu. À Inês, por se ter tornado a minha melhor amiga e a primeira a acreditar em mim mais que eu. Ao Xavi, por toda a admiração que demonstra por mim constantemente e por animar os meus dias com as suas parvoíces. Ao Pedrinho por ter sido o meu acompanhante de viagem nesta aventura e ter acalmado a minha ansiedade vezes sem conta. Ao Pitta, ao Juju, ao meu mano do coração Tomás, ao Nuninho, Martinha, Kika e Ivy pela vossa amizade e amor constantes! Serão sempre imensamente especiais e sem vocês nunca teria conseguido sobreviver estes anos…

Por último e mais importante, um enorme agradecimento à minha família.

Aos meus pais, por me proporcionarem todas as oportunidades para chegar aqui. Ao meu pai, obrigada por seres um exemplo de esforço e sucesso e me teres ensinado que sem trabalho não se chega a lado nenhum e me teres dado o sentido de responsabilidade que tenho o orgulho de ter. À minha mãe, por seres a pessoa mais bondosa do mundo, ouvindo-me e motivando-me sempre que chegava a casa a chorar sem saber se tinha capacidade para isto. Por seres uma mulher incrível, compreensiva, e na qual eu tenho o maior orgulho em chamar de Mãe.

À minha avózinha linda. À minha cunhada Mariana e aos meus irmãos de sangue, Matilde, Pedro e Gonçalo por estarem do meu lado incondicionalmente, e às irmãs que a vida colocou no meu caminho há muitos anos: Matilde, Mariana e Pilar.

A vocês todos, o meu mais sincero obrigada!

ABSTRACT

Currently, cancer is one of the most widespread diseases with related deaths. Conventional treatments such as chemotherapy and radiotherapy are not targeted at cancer cells, leading to serious side effects for the human body. As technology evolves, new possibilities for cancer treatment arise.

In this context, cancer theranostics provides the possibility of having diagnosis and treatment in one only system, improving patient care, and providing customized cancer treatment methods. One of the most promising approaches to theranostics is the use of superparamagnetic iron oxide nanoparticles (SPIONs) as they may be used as contrast agents in magnetic resonance imaging and magnetic hyperthermia, due to the increase of their bulk temperature and their surroundings when an external alternating magnetic field is applied. Not long ago, it was discovered that SPIONs can mimic enzymes such as peroxidase and catalase. Peroxidase-like activity contributes to direct tumour elimination by generating toxic radicals while catalase-like activity leads to conversion of hydrogen peroxide into water and oxygen, helping overcome the hypoxia present in tumour tissues.

In this master thesis, SPIONs were coated with 3-amino-propyltriethoxysilane (APTES) and intercalated into Montmorillonite (MMT) nanoclays, and the resulting composite systems were characterized. The incorporation of magnetic nanoparticles in clays and their catalytic activity enables the development of a potential application for cancer treatment. The enzyme-like activity of magnetic nanoclays was evaluated at given pH values, and the influence of the surface coating on the stability of the composites over a week and a month of storage were assessed. Lastly, SPIONs and magnetic nanoclays were submitted to an alternating magnetic field and hyperthermic temperatures were successfully reached.

The present work demonstrated that these composite systems possess intrinsic catalase and peroxidase-like activities. With a view to medical application of these materials, further studies are required on their cytotoxicity, as well as more in-depth magnetic hyperthermia assays including various iron concentrations. The properties of the magnetic nanoclays produced indicate their potential as a platform for a future application in cancer theranostics.

Keywords: Cancer, Catalase, Montmorillonite, Magnetic nanoclays, Magnetic hyperthermia, Peroxidase, Superparamagnetic nanoparticles, Theranostics

RESUMO

Atualmente, o cancro é a causa de morte com maior incidência em todo o mundo. Os tratamentos convencionais, como a quimioterapia e radioterapia não são direcionados apenas às células cancerígenas, levando a sérios efeitos colaterais para o paciente. À medida que a tecnologia evolui, surgem novas possibilidades para o tratamento do cancro.

Nesse contexto, o teranóstico de cancro oferece a possibilidade de diagnóstico precoce e tratamento num único sistema, melhorando o atendimento ao paciente e disponibilizando métodos personalizados de tratamento de cancro. Assim, uma das abordagens mais promissoras para teranóstico é o uso de nanopartículas superparamagnéticas de óxido de ferro (conhecidas como SPIONs), pois podem ser usadas como agentes de contraste em imagens de ressonância magnética e hipertermia magnética, devido ao aumento da sua temperatura e do ambiente em redor quando um campo magnético alternado externo é aplicado. Mais recentemente, descobriu-se que as SPIONs podem mimetizar enzimas como a peroxidase e catalase. A atividade de peroxidase contribui para a eliminação direta do tumor, gerando radicais tóxicos enquanto a catalase converte o peróxido de hidrogénio em água e oxigénio, ajudando a minimizar a hipoxia presente nos tecidos tumorais.

Nesta dissertação de mestrado, SPIONs foram revestidas com 3-amino-propiltrietoxissilano (APTES) e intercaladas em nanoargilas de Montmorilonite (MMT), e os sistemas compósitos resultantes foram caracterizados. A incorporação de nanopartículas magnéticas nas argilas e a sua atividade catalítica possibilita o desenvolvimento de uma potencial aplicação no tratamento do cancro. A atividade peroxidase e catalase das nanoargilas magnéticas foi avaliada em valores de pH distintos e a influência do revestimento das SPIONs na estabilidade do complexo ao longo de uma semana e um mês de armazenamento em solução foi estudada. Por fim, as SPIONs e as nanoargilas magnéticas foram submetidas a um campo magnético alternado e as temperaturas hipertérmicas foram atingidas com sucesso.

O presente trabalho demonstrou que estes sistemas compósitos possuem atividades intrínsecas semelhantes à catalase e peroxidase. Com o objetivo de aplicar estes materiais na área médica, são necessários mais estudos para avaliar a sua citotoxicidade, bem como ensaios de hipertermia magnética mais aprofundados, incluindo maior concentrações de ferro. As propriedades das nanoargilas magnéticas produzidas demonstram o seu potencial para uma futura aplicação no teranóstico de cancro.

Palavras-chave: Cancro, Catalase, Montmorilonite, Nanoargilas magnéticas, Hipertermia magnética, Peroxidase, Nanopartículas superparamagnéticas, Teranóstico

CONTENTS

ACKNOWLEDGMENTS vii
ABSTRACT ix
RESUMO xi
CONTENTS xiii
LIST OF FIGURES xv
LIST OF TABLES xvii
ABBREVIATIONS xix
INTRODUCTION 1
1.1 Cancer: a worldwide problem 1
1.2. Superparamagnetic iron oxide nanoparticles (SPIONs) 1
1.3. Surface modification of SPIONs 2
1.4. Magnetic hyperthermia 3
1.5. Magnetic nanoclays (MNCs) 3
1.6. Nanozymes and catalytic activity of SPIONs 5
1.6.1. Peroxidase-like activity 5
1.6.2. Catalase-like activity 6
MATERIALS AND METHODS 7
2.1. Synthesis of SPIONs 7
2.2. Spectrophotometric Determination of Iron by UV-Vis 7
2.3. Stabilization of SPIONs with APTES 7
2.4. Preparation of Magnetic nanoclays (MNCs) 8
2.5. Catalytic activity and enzymatic assays 8
2.6. MNCs characterizations 9
RESULTS AND DISCUSSION 11
3.1. SPIONs and magnetic nanoclays characterizations 11
3.2. Magnetic Hyperthermia 21
3.3. Enzymatic assays 22
3.3.1. Nanozyme activity (U) and specific activity (SA) 22
3.3.2. Catalytic activity of NPs and magnetic nanoclays 23
CONCLUSIONS AND FUTURE PERSPECTIVES 29
REFERENCES 33
APPENDIX 37

LIST OF FIGURES

Figure 1 - **Chemical structure of 3-amino-propyl-triethoxysilane** (APTES). 2
Figure 2 **- (A) Structure of MMT**. Adapted from Royal Society of Chemistry, 2023 [16] 4
Figure 3 - Cloisite 10A chemical structure (C10A). 8
Figure 4 - **X-ray pattern of SPIONs and magnetic clays. A)** Naked Fe_3O_4 NPs (a), APTES coated NPs (b)..... 12
Figure 5 – **Scanning electron microscopy micrographs** of **(A)** pristine **MMT**, **(B) OMMT**, **(C) Na116 MNCs**, (**D) C10A MNCs**, **(E) Na116 APTES** and **(F) C10A APTES** MNCs. 14
Figure 6 – **EDS mapping** of carbon, oxygen, silica, aluminium, and sodium for **MMT (a)** and **OMMT** clay **(b)**. 15
Figure 7 - **EDS mapping** of carbon, oxygen, silica, aluminium, sodium, iron, calcium, magnesium, and nitrogen for **Na116 MNCs**. 16
Figure 8 - **Energy dispersive X-ray spectroscopy** spectrum and elements of **Na116 MNCs.** 16
Figure 9 - **Energy dispersive X-ray spectroscopy** spectrum and elements of **Na116 APTES MNCs.** 17
Figure 10 – **ATR-FTIR Spectra of iron oxide nanoparticles and magnetic nanoclays. A)** Naked Fe_3O_4 NPs (a), APTES coated NPs (b). **B)** unmodified MMT NA116 (c), NA116 MNCs (d), NA116 APTES MNCs (e), C10A MNCs (f), C10A APTES MNCs 18
Figure 11 – **TGA curves for: A)** naked SPIONs, APTES SPIONs and **B)** MMT, OMMT and all magnetic nanoclays. 19
Figure 12 - **Temperature variation of naked SPIONs, APTES coated SPIONs and all MNCs** 2.5 mg mL^{-1}. Assays were carried out for 10 minutes at a magnetic flux density of 300 Gauss. The results are expressed as average ± standard deviation for 3 independent experiments. 21
Figure 13 – **Comparison of the SAR values** of pristine NPs, APTES NPs and all magnetic nanoclays. The results are expressed as average ± standard deviation for three independent experiments. 22
Figure 14 – **(A) Colorimetric assay using TMB as substrate for APTES NPs** (1870 µL of 100 mM buffer pH 3.5; 100 µL of 10 mg mL^{-1} TMB; 5 µL of 5 mg mL^{-1} APTES coated SPIONs, 25 µL of 8.8 M H_2O_2) and 24
Figure 15 - **Absorbance spectrum of hydrogen peroxide and NPs.** This assay was carried out using 10 µL of 5 mg mL^{-1} APTES SPIONs and 20 µL of H_2O_2 0.88 M, in 1mL of phosphate buffer (100 mM, pH 6.0)..... 24
Figure 16 – **Assays to assess the catalase-like activity of APTES SPIONs. (A)** 5 µL of APTES SPIONs 5 mg mL^{-1}, 1 mL of phosphate buffer (10 mM, pH 7.4) and 20 µL of 0.88 M H_2O_2. **(B)** Assay carried out using 10 µL of APTES SPIONs 5 mg mL^{-1} and 20 µL of 0.88 M H_2O_2, in 1 mL of phosphate buffer (10 mM, pH 7.4), in a quartz cuvette..... 25
Figure 17 - **Effect of surface coatings on peroxidase-like activity of MNCs.** 5 µL **APTES SPIONs** 5 mg mL^{-1}; 1870 µL sodium acetate buffer (100 mM, pH 3.5); 100 µL 10 mg mL^{-1} TMB; 25 µL H_2O_2 (8.8 M). 26
Figure 18 - **Effect of surface coatings on catalase-like activity of MNCs pH 7.4.** This assay was carried out using a specific quantity of 5 mg mL^{-1} APTES or MNCs, 20 µL of H_2O_2 0.88 M, in 1mL of phosphate buffer (10 mM, pH 7.4). The assays were made in duplicate. 27

Figure 19 - **Effect of surface coatings on catalase-like activity of MNCs pH 6.** These assays were carried out using a specific quantity of 5 mg mL^{-1} APTES or MNCs, 20 μL of H_2O_2 0.88 M, in 1mL of phosphate buffer (10 mM, pH 6). The assays were made in duplicate. 28

LIST OF TABLES

Table 1 - **Energy dispersive X-ray spectroscopy** components wt. % of **MMT and OMMT.** 15
Table 2 - **Energy dispersive X-ray spectroscopy** components wt. % of all **magnetic nanoclays.** 17
Table 3 - **Data from TGA-DSC** analysis characterization for all nanoclays. 20
Table 4 - **Optimized values and quantities used for the buffers**, **MNCs and H_2O_2 for catalase-like activity assays.**..... 25
Table 5 - **Specific peroxidase-like activity values** of APTES coated SPIONs and all magnetic nanoclays at **pH 3.5.**..... 26
Table 6 - **Specific catalase-like activity values** of APTES coated SPIONs and all magnetic nanoclays at **pH 7.4.**..... 27
Table 7 - **Specific activity values** of APTES coated SPIONs and all magnetic nanoclays for **catalase-like activity** at **pH 6.**..... 28

ABBREVIATIONS

NPs	Nanoparticles
MNPs	Magnetic nanoparticles
SPIONs	Superparamagnetic iron oxide nanoparticles
DMSA	Dimercaptosuccinic acid
APTES	3-Aminopropyl-triethoxysilane
MMT	Montmorillonite
OMMT	Organically Modified Montmorillonite
C10A	Cloisite 10A
CAT	Catalase
ROS	Reactive oxygen species
SAR	Specific Absorption Rate
DMSO	Dimethyl Sulfoxide
XRD	X-ray Diffraction
DSC-TGA	Differential scanning calorimetry and thermal gravimetric analysis
DTG	Differential thermogravimetric analysis
EDX	Energy dispersive x-ray spectroscopy
EDS	Energy dispersive spectroscopy
FTIR	Fourier-transform infrared spectroscopy
EE	Encapsulation efficiency
d_{001}	d-spacing/basal spacing
SEM	Scanning electron microscopy

INTRODUCTION

1.1 Cancer: a worldwide problem

Cancer is one of the major health concerns worldwide. Each year millions of people are diagnosed with cancer, being a leading cause of death worldwide. According to the International Agency for Research on Cancer, GLOBOCAN estimates, only in 2020, about 19.2 million new cases of cancer emerged and about 9.9 million deaths occurred due to this disease, all over the world. [1]

One of the most terrific features of cancer is the fast development of anomalous cells that grow beyond their usual limits, spreading fast to other organs. Treatment therapies involve destroying and removing cancerous cells through radio and chemotherapies. Although these are the most used methods, they may not be the most efficient and the destruction of healthy tissues is certain. So, many studies are being made to find the best suitable cancer treatment and theranostics adopting a more innovative method, moving away from conventional therapies, and focusing on targeted therapy. This does not mean that we should leave chemotherapy and radiotherapy, but we can benefit from these complementary methods. In this follow-up, comes the use of magnetic nanoparticles in association with clays for further magnetic hyperthermia studies. These NPs can generate heat by themselves through the application of an alternating magnetic field, thus leading to apoptosis of cancer cells. However, MNPs tend to change their oxidation state and start to agglomerate losing their magnetic properties as time goes on. To overcome this issue, it is essential to use two-dimensional layered materials such as clay minerals to give them stability, better magnetization, and durability. [2]

In this master dissertation, a therapy for cancer was suggested developing a multifunctional system based on the combination of superparamagnetic iron oxide nanoparticles with montmorillonite clays. The main goal was the development and detailed characterization of SPIONs to proceed to its encapsulation in clays for later magnetic hyperthermia and catalytic activity assays. The enzymatic activity influence of these magnetic nanoclays will be assessed and hyperthermia assays will provide information on their heating ability.

1.2. Superparamagnetic iron oxide nanoparticles (SPIONs)

Magnetic nanoparticles (MNPs) are a type of nanoscale material characterized by its small dimensions, between 1 and 100 nm, having the ability to respond to a magnetic field. They have generated significant interest in recent years having wide potential and practical applications in magnetic hyperthermia for cancer therapy, drug delivery, as contrast agents for magnetic resonance imaging (MRI) and more. [2] Metallic NPs have larger magnetization compared to metal oxides, but they are not stable in air and are easily oxidized. From all iron oxide nanoparticles, the most common biocompatible magnetic nanomaterials are pure oxides, magnetite (Fe_3O_4) and maghemite (γ-Fe_2O_3). [4] [5]

Superparamagnetic iron oxide nanoparticles, commonly known as SPIONs, are the only clinically approved metal oxide nanoparticles showing the most interest in these last decades due to its enormous potential, particularly, on the biomedical field. Their stable storage in the colloidal suspensions and their simple preparation process become great advantages. Colloidal suspensions of stabilized magnetic nanoparticles are called ferrofluids which can interact with a magnetic field. [3] [6] These particles show interest as they have exceptional properties of superparamagnetism that confers advantages such as the generation of heat, which results the alternating magnetic field or the capability to be guided to a specific tissue or organ by an external magnetic field.

Common to all NPs, SPIONs have unique physicochemical properties due to their nanometer size (only referred as SPIONs when the critical size is below 15 nm), easy of synthesizing and large surface area, which on the other hand could become a problem. For example, large surface area along

with amplified reactivity may induce cytotoxicity that can impair the functions of key cell components, namely mitochondria, nucleus, and DNA. [7] However, all of this are still under investigation, but such applications have exploited more advantages than disadvantages. Iron oxides show low toxicity to human beings and its magnetization can be easily controlled. It is well recognized that optimizing the physicochemical parameters is highly effective to minimize the immune response and toxicity of SPIONs. Parameters such as charge, surface coating, and morphology, influence the efficacy of SPIONs and their biomedical fate within cells. Proper surface coatings can stabilize iron oxide NPs and avoid agglomeration and oxidation. It is also an efficient way of preventing the dissolution and release of toxic ions. [8]

Iron oxide NPs consists of a single magnetic domain (in the superparamagnetic state the magnetic moments are all magnetized in the same direction and do not have the presence of any domain walls due to the absence of hysteresis cycles). Due to this behaviour, as mentioned before, the NPs are easily magnetized under the application of an external magnetic field and demagnetized once that field is removed showing no traces of magnetization. [7] Although having all these advantages, the iron oxide NPs are unstable in solution and tend to suffer agglomeration losing their superparamagnetic properties. Controlling the stability of ferrofluids against this is crucial because the formation of aggregates modifies their specific surface area and dispersibility as well as influence their efficiency as a drug vehicle. [2] To prevent these circumstances, they need to be coated and stabilized. The coating can be made with various materials like polymers, metals, etc, but it can also be used with surfactants such as dimercaptosuccinic acid (DMSA) or 3-amino-propyl-triethoxysilane (APTES). [3] [5]

1.3. Surface modification of SPIONs

Uncoated SPIONs have extremely low stability that can lead to precipitation (if not sufficiently small) due to gravitation forces and a high rate of agglomeration under some physiological conditions, being non-effective for any clinical application. Naked NPs are stable in high-and-low suspensions, but not in neutral pH so they must be coated for various reasons: to increase their stability and protect against aggregation; allow molecule binding; defend the magnetic core from oxidation; to provide a reactive surface to allow their functionalization; to protect NPs against reticuloendothelial system (RES) uptake and elimination in order to enhance the blood circulation time and, lastly, to avoid the generation of reactive species of oxygen upon exposure of cells to the SPIONs, preventing cytotoxicity effects. [8] [9]

Thus, the surface of SPIONs can be modified through the formation of atomic layers of some organic or inorganic molecules. It is common to use a chelating agent which is a chemical compound that reacts with metal ions to form stable water-soluble complex. For example, meso-2,3-dimercaptosuccinic acid (commonly known as DMSA) contains two sulfhydryl groups (-SH) and can be used as a biocompatible stabilizer coating for MNPs. Also, alkoxysilanes can be used to modify the surface of SPIONs such as 3-amino-propyl-triethoxysilane (APTES) that will be the alkoxysilane used in this work. [9] - [11] 3-Aminopropyl-triethoxysilane (APTES), $C_9H_{23}NO_3Si$, chemical structure is represented in **Figure 1**.

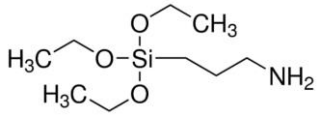

Figure 1 - **Chemical structure of 3-amino-propyl-triethoxysilane** (APTES).
Adapted from Sigma-Aldrich website 2022

Bini *et al.* showed that ethyl groups grant larger steric stability to ferrofluids reducing the aggregation of SPIONs, being the main reason why it was selected as an important surface coating for

this work and due to lack of information regarding magnetic nanoclays with APTES coated SPIONs. [3]

1.4. Magnetic hyperthermia

The preferential killing of cancer cells without damaging normal tissues has been a desired goal in cancer therapy for many years. However, procedures such as chemotherapy or radiotherapy tend not to be the most effective way of achieving this target. This way, magnetic hyperthermia is a promising technique for cancer treatment, performed using heat as a therapeutic agent to induce the death of tumor cells. The potential of hyperthermia was first predicted following observations that cancerous cells have a lower heat tolerance than the healthy cells, estimated to reach their limit at approximately 42 ºC, while healthy cells can reach higher. [25] [26] Therefore, this type of therapy has fewer side effects on the patient healthy cells when compared to the conventional ones.

Recently, SPIONs have gained attention due to their ability to induce magnetic hyperthermia. The NPs are dispersed in the tumor area and an external magnetic field is applied. These particles can convert electromagnetic energy into heat through the application of an alternating magnetic field and cause the apoptosis of cancerous tissues. This alternating magnetic field gives the NPs enough energy to overcome the reorientation energy barrier. When the magnetic moments return to their equilibrium state, energy is dissipated resulting in the heating of the NPs by Brownian rotation and Neel relaxation. Brownian rotation and Neel relaxation, are, respectively, the result of the rotation of the NPs and the rotation of their magnetic moments. [27] [28] In magnetic hyperthermia, there is a primarily interest in the thermal effect. The rate of temperature increase, and the final temperature distribution are the determining factors of a successful treatment. Researchers have adopted the Specific Absorption Rate (SAR) defined as the quantity of power absorbed by the sample as per mass unit ($W.g^{-1}$) (**Equation 1**). [29] [30]

$$\mathrm{SAR} = \frac{C_{NP} m_{Fe} + C_l m_l}{m_{Fe}} \left(\frac{dT}{dt}\right)_{max} \quad (\mathrm{W\ g^{-1}}) \qquad \textbf{Equation 1}$$

where $(dT/dt)_{max}$ is the maximal gradient of temperature curve, C_{NP} is the specific heat of the magnetite nanoparticles (0,16 kCal/kgºC), C_l is the specific heat of the liquid (1.0 kcal/kg ºC), m_l is the fluid mass, and m_{Fe} is the iron mass in the colloid. [5] [31] For this reason, SPIONs applied to magnetic hyperthermia and possibly magnetic nanoclays are appealing as they offer a way to ensure only the intended target tissue is heated.

1.5. Magnetic nanoclays (MNCs)

Two-dimensional layered materials such as clay minerals are biocompatible and present great physicochemical properties for drug delivery systems. By having interlayer spaces, clays provide an accommodate location to nanoparticles, thus offering them stabilization and contributing to enhancing the resulting nanocomposite properties.

Clays fundamentally contain silicon, aluminium or magnesium, oxygen, and hydroxyl groups with various associated cations. These ions and OH groups are organized into two dimensional structures as sheets. Clay mineral structure is composed of 2 principal units: tetrahedral silica (T) and octahedral alumina (O) sheets. They can be classified into 1:1 and 2:1 type according to the layering of T and O sheets. The 1:1 clay consists of a single T sheet linked to a single O sheet, and 2:1 clay consists of a single O sheet between two T sheets creating a Vander Waals gap between layers. These aluminosilicate layers have an overall negative charge, due to isomorphic substitutions in the O and T sheets, which is counterbalanced by exchangeable metal cations such as Na^+, $Ca^{2+,}$ $Mg^{2+,}$ Fe^{2+} and Li^+ residing in the

interlayer space, as well as water molecules. Montmorillonite (MMT) is a 2:1 clay mineral with two tetrahedral sheets of SiO_4 and one octahedral Al_2O_3 sheet in between, described by the unit cell formula $[Al_2(OH)_2(Si_2O_5)_2]$. [12] - [14]

MMT is the most used phyllosilicate mineral and one of the major constituents of Bentonite used for biomedical purposes. This type of clay belongs to the smectite family, which is characterized by their surface reactivity and low layer charge that allow their particles undergo complete dissociation in water and give them interesting properties. Also, MMT shows extensive interlayer expansion, high specific surface area, high cation exchange capacity and contributes to enhancing the resulting nanocomposite. The space within the clay layer is called interlayer spacing and the height of each layer is about 1 nm. The thickness of each repeating unit (one clay layer and one interlayer spacing) is known as the basal spacing or d-spacing (d_{001}). In addition, clays' layers allow many strategies as intercalating, pillaring, supporting and encapsulating which can be well employed to isolate, accommodate and stabilize individual MNPs. [13] - [15] A schematic structure of the MMT [16] and surface modification of MMT is shown in **Figure 2.** [40]

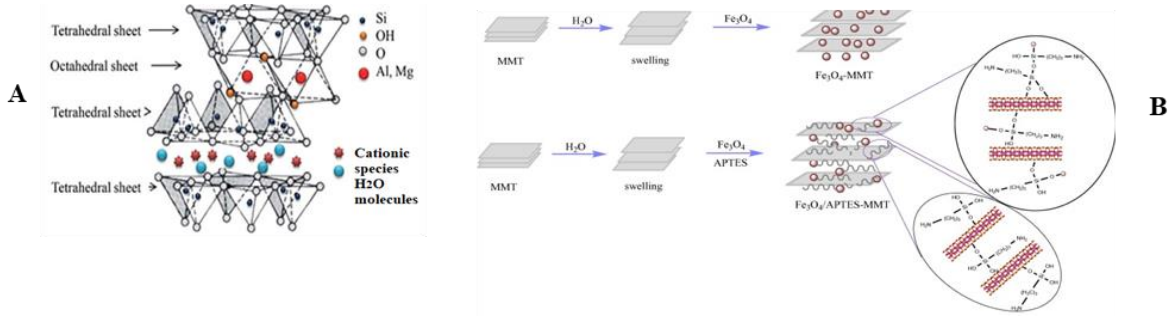

Figure 2 - **(A) Structure of MMT**. Adapted from Royal Society of Chemistry, 2023 [16]
(B) Schematic of surface modification of MMT [40]

Intercalated nanocomposite is formed when the MNPs successfully penetrate the interlayer spacing of the layered silicate significantly expanding the interlayer spacing (with a d_{001} of approx. 2 to 3 nm) while maintaining their clay properties. [12] [13] The isomorphous substitution of Al^{3+} with Mg^{2+} or Fe^{2+} results in negative surface charge of MMT layers', which is balanced by interlayer cations. High cation exchange capacity and swelling ability of MMT particles allow them to intercalate drug molecules and others into the interlayer space and release them afterwards by replacement with cations present in the release media. Moreover, when the clay platelets are completely separated and disorientated from each other exfoliated nanocomposites are obtained, even though completely exfoliated structures are not usual. [16] Therefore, clay reinforcement with NPs offers a possible solution to enhance its integrity, controlling drug release kinetics and optimize its bioactivity and theranostics capacity. Encapsulating drugs into nanoclays' interlaminar space might be an effective strategy to address the challenge of prolonged dosing regimens and subsequent enhanced therapeutic by keeping the active agent concentration in the local targeted environment. [12] [13] [15]

In this work, pristine MMT and a commercially available organically modified MMT will be used to evaluate the most adequate nanoclays to incorporate MNPs. The major inconvenience of pristine MMT is their high hydrophilicity due to its high surface energy and strong cohesive interaction between nanoclay layers which makes them incompatible with a wide range of organic and non-polar polymers. [13][14] Therefore, there is a need to make it more compatible so the clay should be modified with an organic modifier to organophilic, as displayed in **Figure 2 (B).** As previously referred, it will be used the pristine MMT (Nanofil 116/Na116) and organo-modified MMT currently available with the commercial name of Cloisite 10A (more known as C10A).

1.6. Nanozymes and catalytic activity of SPIONs

Enzymes are vital to all biological processes such as detoxification, metabolism and biosynthesis and when a defect occurs leads to metabolic disorders and increases the risk of several adverse effects. Although, damages caused by enzymes can act against tumour growth. In aerobic forms of life, the production of energy generates H_2O_2 and other reactive oxygen species which can be toxic to the system. [17] [18] H_2O_2 has been found to be part of the cell's signalling cascade when in low concentrations but can be very toxic when in high concentrations. As a form of stabilizing and dissociating these ROS, eucaryotic cells develop antioxidant enzymes. Catalase (CAT) is the major enzyme that can be found in the peroxisomes of animal cells and plays a critical role in tumour therapy as it is essential for neutralizing harmful ROS such as H_2O_2. [19]

As it is known, the tumour area is very rich in hydrogen peroxide due to hypoxia and its acidic extracellular pH. So, catalase can convert this molecule into water and oxygen and improve conventional cancer therapies. Nonetheless, clinic implementation of enzymes is very limiting due to enzymes high susceptibility to denaturation effects induced by temperature, pH, and degradation. [20] Recent studies from *Gao et. al* found the first enzyme-like activity in ferrous nanomaterials. The iron oxide nanoparticles Fe_3O_4, can mimic some enzymes being considered as a new form of artificial enzymes, possessing intrinsic peroxidase-like activity with catalytic behaviour. In this article *Gao et al*. compared the activity of horseradish peroxidase (HRP) and Fe_3O_4 NPs through enzymatic assays (oxidation of substrates; pH, H_2O_2 concentration dependence; etc) and in the end was able to say that Fe_3O_4 NPs beyond doubt have intrinsic peroxidase-like activity and are similar to the HRP enzyme. [17]

Iron oxide enzymes (Ionzymes) display two types of enzymatic activity under physiological conditions: peroxidase-like activity and catalase-like activity. Both enzymes use the same molecule as substrate, hydrogen peroxide (H_2O_2), having only a difference on the generated product. Peroxidase converts the substrate into water and free radicals to react with a hydrogen donor and catalase generates oxygen and water as seen by the chemical reactions below **(Equation 2)**:

Equation 2

$$\underset{\text{Peroxidase}}{H_2O_2 + 2AH \rightarrow 2A + 2H_2O} \qquad \underset{\text{Catalase}}{2H_2O_2 \rightarrow O_2 + 2H_2O}$$

Moreover, Chen *et al.* produced γ-Fe_2O_3 and Fe_3O_4 NPs coated with DMSA to evaluate the intrinsic enzyme-like activity of SPIONs. [22] To evaluate the intrinsic enzyme-like activity of SPIONs for peroxidase-like activity it was used 3,3',5,5'-tetramethylbenzidine (TMB) as hydrogen donor in the presence of hydrogen peroxide. Both types of nanoparticles, naked or coated, were able to catalyse the oxidation of TMB as the color of the reaction media changed immediately to blue after adding the nanoparticles to the reaction system. [17] [21] [23] However, Chen *et al.* showed evidence of higher peroxidase-like activity for Fe_3O_4 NPs under the same circumstances. When the pH was 7.4, the H_2O_2/TMB remained transparent with both nanoparticles, revealing that the NPs do not exhibit peroxidase-like activity under neutral pH conditions. Nonetheless, the researchers found that under pH 7.4, they possess catalase-like activity as several minutes after adding H_2O_2 into Fe_3O_4 nanoparticles diluted in a phosphate buffer, gas bubbles were observed. [22] Knowing this, it is predictable that magnetic nanoclays show some catalytic activity as well.

1.6.1. Peroxidase-like activity

To evaluate the peroxidase-like activity of magnetic nanoclays with hydrogen peroxide as a substrate, usually the consumption of H_2O_2 and the formation of the oxidized substrate are studied. It is often used a colorimetric method with TMB as a hydrogen donor. TMB is oxidized and produces a blue color in the reaction system. [17] [23]

1.6.2. Catalase-like activity

As there is lack of information regarding catalase-like activity in nanoclays solutions, there was a need to carry some experiments to assess if there is possible to measure the activity at 240 nm, because of H_2O_2 decomposition. The shift between catalase or peroxidase-like activity depends on the physiological conditions, pH, or temperature, but most likely has to do with the pH. When the environmental pH changes to neutral or basic, the Fe^{3+} content in the iron-based nanozymes becomes the dominant catalytic species, favouring the catalase-like decomposition of H_2O_2. [20]

First, for this evaluation H_2O_2 consumption and molecular O_2 formation are assessed. The reaction between catalase and H_2O_2 is visible by itself to naked eye due to gas bubbles formation, which does not affect the measurement. Aforementioned, catalase-like activity is found to be more preponderant in neutral or basic pH conditions, more precisely a pH around 7.4, showing no relevant expression compared with peroxidase-like activity. [17] [24]

MATERIALS AND METHODS

2.1. Synthesis of SPIONs

The iron oxide nanoparticles (SPIONs) used in this work were synthesized by chemical co-precipitation method, according to a protocol (detailed in **Appendix A.1**) by Soares *et. al* [5], using the following precursors: $FeCl_3.6H_2O$: 5 mmol (*Alfa-Aesar*); $FeCl_2.4H_2O$: 2.5 mmol (*Sigma-Aldrich*) dissolved in 10 mL and 2.5 mL of milliQ water, respectively. Also, 50 mL of milliQ water was added to the iron mixture to obtain a molar ratio of 1:2 (Fe^{2}+: Fe^{3}+). The deaeration of O_2 from the solution is made with bubbling N_2. The reaction is initiated after rapidly adding 10 mL of ammonia solution and the process is kept for 5 minutes, after which it is stopped by adding 60 mL of deionized water. The SPIONs precipitate is washed five times and left to settle by magnet separation then the top water layer is discarded.

2.2. Spectrophotometric Determination of Iron by UV-Vis

The concentration of iron present in the NPs solution was determined using the 1,10-phenanthroline colorimetric method based on *Talelli et al.* 2009 and *Soares et al.* 2014 detailed on **Appendix A.1.1.** [5] [10] Primarily, 40 μL of the diluted SPIONs suspension was placed into five Eppendorf tubes followed by addition of 20 μL of HCl 37% (v/v) (*Panreac*) and then, incubated for 1 hour at room temperature to dissolve all the NPs and obtain ferrous and ferric chloride. Following this, 100 μL of hydroxylamine hydrochloride (*Sigma-Aldrich*) solution 100 mg mL^{-1} (previously prepared in 0.01 M HCl) was added to reduce Fe (III) to Fe (II) and 500 μL of 1,10-phenantroline monohydrate (*Sigma-Aldrich*) solution 3 mg mL^{-1} to achieve the orange-red complex of tris(1,10-phenanthroline) iron (II). To end, the samples were diluted to 1800 μL by adding ammonium acetate (*Panreac*) 500 mM pH 4 buffer. The last two solutions were, also, previously prepared in 0.01 M HCl as it serves as a solvent for all of them.

Lastly, the samples light absorbance at 510 nm (at which Fe (II) most absorbs) is measured in a UV-VIS Spectrophotometer (T90+ UV/VIS Spectrometer PG Instruments Ltd) using a HCl 0.01 M solution as "blank". Values obtained (Abs) are the input in a calibration curve (Abs=4.5079 [Fe]+0.0753) to determine Fe (II) concentration. Thereafter, the formula [Fe] = 0.7 x [NPs] was used to obtain the nanoparticles concentration and the ratio was obtained from control experiments.

2.3. Stabilization of SPIONs with APTES

APTES was selected as an important surface coating since its ethyl groups grant more considerable steric stability onto the ferrofluids, reducing the aggregation of SPIONs and because of their few studies as a surface coating for MNCs. For this purpose, an adapted method from *Mashhadizadeh et al.* was used. [32] Stabilization with APTES was done after washing the NPs. Thus, 20 mL of a 10% (v/v) aqueous solution of APTES (*Merck*), and 10mL of glycerol (*Pharmaceutical glycerin)* to prevent water evaporation was added to the NPs suspension. The mixture was heated in an oil bath at 90◦C under mechanical stirring (~500 RPM) for 2 hours. After waiting for the suspension to cool at room temperature, it was washed five times following the sequency: water, ethanol, water, ethanol, and water. Finally, the obtained APTES Fe_3O_4 coated SPIONs were dispersed in deionized water and retained on a falcon tube to further characterization and studies.

2.4. Preparation of Magnetic nanoclays (MNCs)

Nanofil 116 and commercial OMMT such as Cloisite 10A from *Rockwood Clay Additives*, were used to produce the desired magnetic nanoclays. The chemical structure of Cloisite 10A (C10A) is displayed in **Figure 3**, where N+ denotes a quaternary ammonium salt; T and HT denote tallow and hydrogenated tallow, respectively. [13]

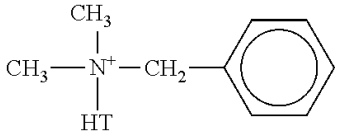

Figure 3 - Cloisite 10A chemical structure (C10A).

To prepare the MNCs, an adapted method from S. Bazgir, A. Rashidi *et al.* (2020) was used [33]. 2 wt.% clay suspension of C10A and Na116 was first prepared at room temperature by adding a specific amount of clay powder, 510 mg, to 25 mL of miliQ water, followed by magnetic stirring for 24 h. Then, to the clay suspension was added 20 wt.% of the SPIONs solution (naked and APTES coated) and milliQ water to make a total amount of 50 ml solution, putting under magnetic stirring for 48 h to guarantee full homogenization and encapsulation of SPIONs into clays. The amount that needs to be added to the clay suspension is calculated based on the iron concentration in the NPs solution. At the end of the process, the magnetic nanoclays solution underwent centrifugation to separate the solid from the liquid phase (supernatant) using a *Fiberlite™ F15-8 x 50cy* centrifuge for 30 min at 10.000 rpm and 20 ºC of temperature followed by lyophilization (freeze-dried by a *VaCo 2 from Zirbus Technology*). The supernatant was removed remaining the solid phase only in the falcon tube, which went to 2 days to lyophilization to completely dry.

2.5. Catalytic activity and enzymatic assays

As mentioned before, NPs catalytic activity and intrinsic ability to generate reactive oxygen species can be used to mimic the catalytic activity of natural enzymes. So, an adapted protocol from Gao *et al* [17] [22] was used to evaluate the peroxidase-like and catalase-like activity of NPs and MNCs. Also, it was studied the effect of the surface coating modification with APTES on both activities since there is almost no information on catalytic activity regarding magnetic nanoclays.

2.5.1. Peroxidase-like activity assays

The peroxidase-like activity tests were carried out in 3 mL plastic cuvettes, where to 2 mL sodium acetate buffer (100 mM, pH 3.5) were added 5 μL and 10 μL of a fixed 5 mg mL^{-1} NPs and MNCs suspension, respectively. It is important to notice that between each measurement the cuvette needed previously agitation, with the assistance of a parafilm sheet, due to iron oxide easy aggregation issues. As the substrate, it was used a given amount of 10 mg mL^{-1} of TMB (*Sigma-Aldrich*) in the presence of 25 μL H_2O_2 (8.8 M). It should also be noted that the concentration of the NPs refers to the concentration of the ferrous nucleus and the coating, whether a coating is or is not present.

To prepare sodium acetate buffer, it was used acetic acid *(glacial*) and sodium acetate anhydrous stored in the fridge and always used fresh and the pH adjusted to 3.5. TMB solution was prepared dissolving the substrate in DMSO (Dimethyl Sulfoxide) and stored in a freezer, acting as a hydrogen donor for the reduction of hydrogen peroxide enzymes. This will cause an immediate color change to blue in the reaction system. [23]

Also, as it is photosensitive it was always kept away from direct sunlight and H_2O_2 was directly used from the bottle. The absorbance was measured using a UV-VIS spectrophotometer (GENESYS 50

UV-Vis Spectrophotometer Thermo Fisher Scientific) at 652 nm for 3 minutes. To minimize the errors inherent to a single reading, all the assays were made in duplicate.

Within this research work objectives', the magnetic nanoclays should retain some peroxidase and catalase-like activities. Therefore, and unless otherwise stated, the peroxidase-like and catalase-like activities of the MNCs in aqueous suspensions were assessed, over a week and a month of storage, as well as the stability of these activities.

2.5.2. Catalase-like activity assays

For catalase-like activity assays, it was used a quartz cuvette of 1 mL of phosphate buffer (10 mM pH 7.4 and 10 mM pH 6) where 5 μL of a 5 mg mL^{-1} solution of naked SPIONs was added in the presence of 20 μL of hydrogen peroxide (0.88 M) showing no activity as stated before. [22] The phosphate buffers were prepared using sodium phosphate monobasic monohydrate ($Na_2HPO_4 \cdot H_2O$) (*Sigma-Aldrich*) and di-sodium hydrogen phosphate heptahydrate (Na_2HPO_4. 7 H_2O) (*Merck*). After these experiments, it was crucial to adjust some parameters of the NPs solutions and H_2O_2, to observe a decrease in absorbance in time, to calculate catalase-like activity for APTES SPIONs and MNCs. Some factors needed to be considered as the spectrophotometer system could not read highly saturated samples, so it was necessary to adjust the volume of NPs in the cuvette as they were more saturated than MNCs and optimize the quantities for each one of them as they presented different behaviours. Those optimized values are described on **Table 4.** The concentration of the solution should be enough to start the conversion of H_2O_2 into oxygen and water. Again, between each measurement the cuvette was previously agitated.

As stated before [17] [21] [23], peroxidase-like activity is way much faster showing expression than catalase, so the assays were made for a longer time, 5 minutes, in duplicate to minimize errors. The absorbance was measured at 240 nm using a 50 UV-Vis Spectrophotometer Thermo Fisher Scientific.

2.6. MNCs characterizations

X-ray Diffraction (XRD) measurements were performed on X'Pert PRO PANAlytical diffractometer, in the range $1^o<2\theta<10^o$ to determine the d-spacing of the nanoclays using a Cu Kα radiation, generated at 45 kV and 40 mA. Transform Infrared (FTIR) Spectroscopy spectra of the nanoclays were obtained using a Nicolet 6700-Thermo Electron Corporation Attenuated Total Reflectance-Fourier Transform Infrared spectrometer (ATR-FTIR) with a resolution of 2 cm^{-1}, in the 4000-400 cm^{-1} wavenumber range. Differential Scanning Calorimetry and Thermal Gravimetric Analysis (DSC-TGA) measurements were made using a Thermal Analyzer NETZSCH STA 449 F3 Jupiter to study the decomposition and weight loss stages, in function of temperature, of all nanoclays used in this work. The heating rate was 10ºC/min, from ambient temperature to 900ºC using a N_2 atmosphere. Scanning Electron Microscopy (SEM) was used to observe the surface morphology of all samples of MNCs produced using Carl Zeiss Auriga's equipment. EDS was also performed with the same equipment using the software Quantax 70 EDS, and it helped identify the chemical elements present in the samples. Also, magnetic hyperthermia studies were performed using the equipment *nB NanoScale Biomagnetics, D5 Series*, and the measurements lasted 10 minutes, with a magnetic flux density of 300 Gauss and a frequency of 388.40 kHz. Three tests for each sample were made to get a more precise analysis.

RESULTS AND DISCUSSION

3.1. SPIONs and magnetic nanoclays characterizations

As mentioned before, NPs were synthesised by chemical co-precipitation and then intercalated into MMT clays. After this, they were characterized to confirm their morphological, structural, and chemical properties.

XRD allows the evaluation of the crystalline structure of the NPs and MNCs confirming which species were obtained for each condition by identifying the characteristic peaks. The X-ray diffractogram of the NPs and MNCs produced is shown in **Figure 4.** For naked Fe_3O_4 SPIONs, the diffractogram **(Figure 4 (A)(a))** shows the presence of six characteristic peaks at 2θ values of 30.3º, 35.6º, 43.4º, 53.4º, 57.3º, and 63.0º, which correspond, respectively, to the diffraction planes (2 2 0), (3 1 1), (4 0 0), (4 2 2), (5 1 1) and (4 4 0) of maghemite and magnetite powders. When comparing this pattern to the standard diffraction spectrum of magnetite powders (code: JCPDS 00-019-0629), it is possible to confirm that the NPs possess a crystalline cubic structure corresponding to magnetite.[5]

Through **Figure 4 (A)(b),** it is also possible to say that after surface modification with APTES coating the characteristic peaks did not change, so the crystalline structure was not compromised. Magnetite and maghemite present their characteristic peaks at similar values of 2θ, making it hard to differentiate the two phases. However, knowing that the reaction was performed under anaerobic N_2 atmosphere to prevent uncontrollable oxidation of Fe^{2+} into Fe^{3+}, it can be affirmed that the NPs are mainly constituted by magnetite, as expected. [34]

The average grain size, τ, can also be calculated through the most intense peak, corresponding to the (311) plane. It can be calculated using Scherrer's equation.

$$\tau = \frac{K\lambda}{\beta \cos(\theta)} \qquad \textbf{Equation 3}$$

Where K is the grain shape factor (K = 0.94); λ is the incident X-ray wavelength (λ= 1.54 Å); β denotes the full width at half-maximum (in radians) of the highest intensity, and θ is the corresponding diffraction angle. The average crystallite size obtained for naked SPIONs was 8.7 nm (2θ = 35.56º) and for APTES stabilized SPIONs was also 8.7 nm (2θ =35.69º). [35]

XRD provides information on the basal spacing (d_{001}) of nanoclays identifying whether the pristine MMT has been successfully modified or not by iron oxide nanoparticles. By considering Bragg's law **(Equation 4)** it was estimated the basal spacing of the nanoclays showing whether intercalation or exfoliation occurs.

$$(2d\sin\theta = \lambda) \qquad \textbf{Equation 4}$$

where d is the distance between the crystallographic planes, θ is the half-angle of diffraction and λ is the wavelength of the X-ray radiation.

The peaks in the graphs (2θ) are attributed to the lamellar arrangement of clay platelets. The expansion of the clays basal spacing, which means an increase of d_{001} values, is confirmed by the shifting of the diffraction peaks towards smaller angles meaning that the modification of nanoclays was achieved. Therefore, by **Figure 4 (B) and (C)** it is possible to observe that all magnetic clays show visible peaks, and the peak positions shift relatively to lower angles when compared to natural occurring montmorillonite which contains exchangeable cations of primarily Na^+. For the unmodified MMT sample, all the observed peaks are close to the characteristic data of Na^+ MMT (JCPDS card No.13-

0135). [36] The typical diffraction peak of MMT usually appears at approximately at 2θ = 6º. In this work, the basal spacing of the unmodified MMT was found to be 1.27 nm at 2θ = 6.93º.

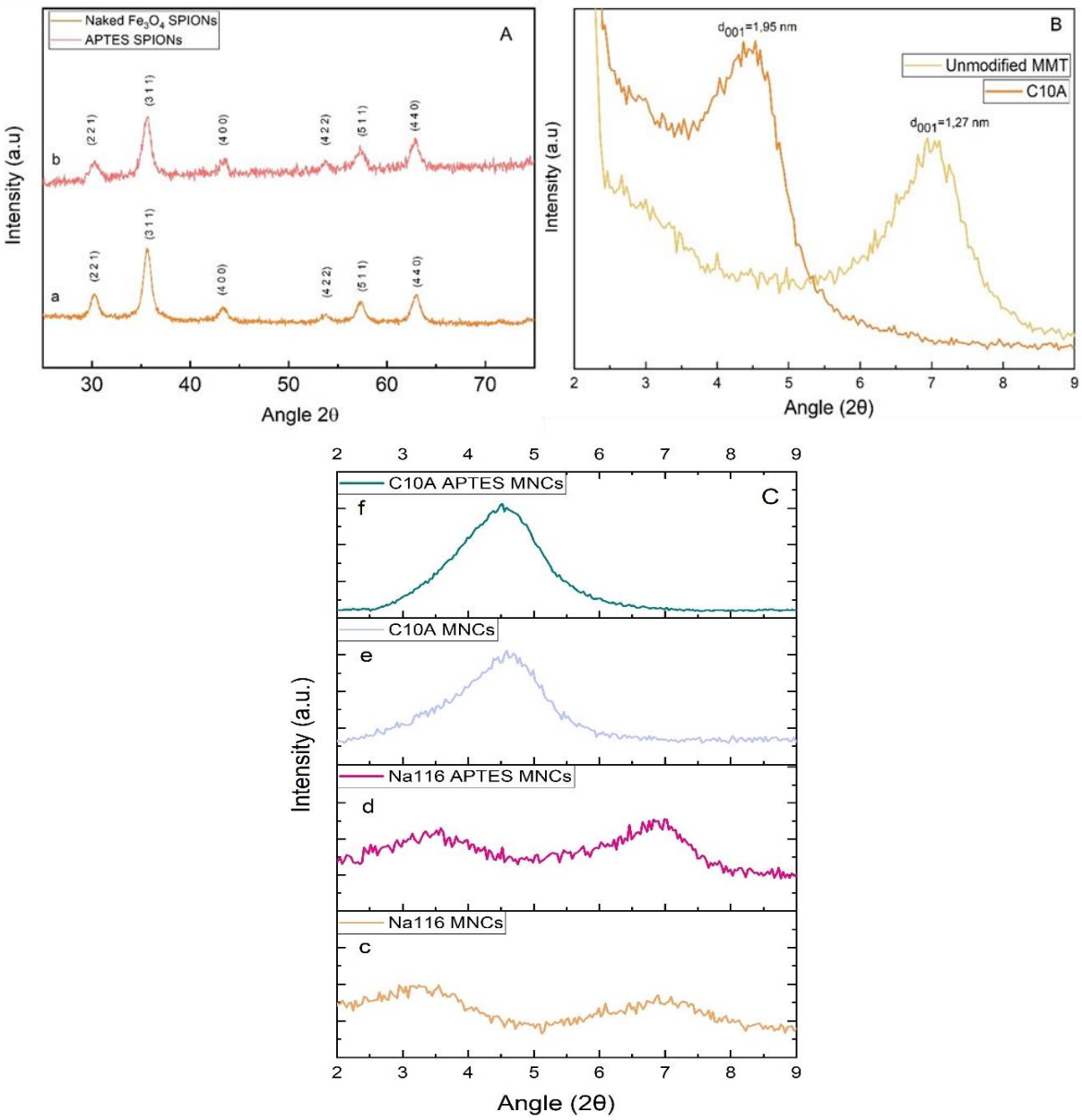

Figure 4 - **X-ray pattern of SPIONs and magnetic clays. A)** Naked Fe_3O_4 NPs (a), APTES coated NPs (b). **B)** unmodified MMT NA116, organically modified C10A, **C)** NA116 MNCs (c), NA116 APTES MNCs (d), C10A MNCs (e), C10A APTES MNCs (f).

Combination with Fe_3O_4 NPs showed two diffraction peaks, **Figure 4 C (c),** the first one is attributed to the presence of NPs into the clays (2θ=3.5º) and the other one to the MMT characteristic pattern. The d spacing of Na116 MNCs was expanded to 1.28 nm at 2θ = 6.88º, showing that the structure of MMT interlayer increased after loading Fe_3O_4 NPs. These results demonstrate that iron ions penetrated the interlayer space of montmorillonite indicating that a cationic exchange occurred between Fe^{3+}/ Fe^{2+} and Na^+ in the layers of pristine MMT, resulting in clay hydration and swelling. Thus, it is possible to say that an intercalation occurred in Na116 clays due to the presence of NPs' peak at 2θ= 3.5º.

Also, the relative reflection intensity of both types of magnetic nanoclays have decreased compared to MMT which means that the highly ordered parallel lamellar structure of the clay was disrupted by the NPs (its (0 0 1) planes are more disordered). Therefore, the iron oxide particles might be dispersed on the external surface of MMT instead of being exclusive in the interlayers. [37]

After modification by APTES Fe_3O_4 NPs, (**Figure 4 C (d),** the basal reflection of Na116 MNCs did not change noticeably, as well as the NPs' peak (2θ=3.5º), but the MMT characteristic peak was shifted to lower angle (2θ = 6.85º) and the basal spacing of Na116 APTES MNCs was 1.29 nm. The values of d spacing are quite similar so the differences between the diffractograms are tenuous, probably due to a small concentration of APTES NPs in the clays. This phenomenon suggests that the layers of Na116 MNCs were partially intercalated by APTES NPs even though the differences are very little.

Regarding the Cloisite 10A, when MMT is modified by an organic modifier the gallery is intercalated and expanded by the molecular chain of the organic modifier becoming more hydrophobic. **Figure 4 B** shows the OMMT with a diffraction peak at 2θ = 4.52º with a d spacing of 1.95 nm, corresponding to the characteristic data of these clays. When adding NPs, (**Figure 4 C (e)),** the characteristic peak shifted to lower 2θ value, 4.5º, meaning the interlayer distances slightly increased resulting in intercalated structures. Also, diffraction peak associated with C10A APTES MNCs was lower at 2θ = 4.48º with a basal spacing of 1.97 nm. This shows that the modification of C10A clay with APTES NPs results on grafting silane in the layers of MMT and the increase of d_{001} also confirmed that APTES molecules were not only grafted on the external surface of MNCs but also intercalated in the layers.

Therefore, it is noticeable there were not significative changes for C10A and C10A APTES magnetic nanoclays in their basal spacing, even though intercalation has been achieved to some extent. However, it is not possible to say there was a complete intercalation of these MNCs. An increase in NPs' solution concentration would accordingly increase the basal spacing of the clay achieving larger distances between the aluminosilicate layers. [38]

The shift of an XRD peak to a lower angle is not sufficient to identify a material as intercalated and this requires SEM-EDS for characterization. The microstructures and morphologies of the samples were characterized by the available SEM tabletop with a magnification of x 3000. **Figure 5** shows SEM images of pristine MMT, OMMT and Fe_3O_4 NPs with or without coating of APTES in the interlayer space of both types of clay. A general view of pristine MMT with a typical sheet-like structure with large flakes can be observed by **Figure 5 (A).** Even though, the images are not very revealing, MMT presents a layered structure with irregular edges and a relatively smooth surface. In the OMMT image on **Figure 5 (B)**, the changing in morphology is quite evident. The clay particles showed themselves more exfoliated due to the organophilization process. MMT was a regular compact solid, clustered with crystalline features, whereas OMMT appeared to be loose flake-like aggregate overlaid or stacked with exfoliated layers. [59]

Figure 5 (C)-(F) shows that the Fe_3O_4 NPs are closely immobilized on the MMT or OMMT surfaces, and it is, also, observed the small differences between morphology structures with or without APTES coating. The regular structure of the clays did not substantially change, only an increased surface roughness result of the chain interactions between the molecules of the clays and NPs. Although, the different brightness of pristine clay and the magnetic nanoclays is due to the presence of Fe_3O_4 NPs and some disordering in the MMT structure given by the abundance of iron oxide on its surface.

One may observe that there are some fine particles on the fractured surface of C10A MNCs, **Figure 5 (D)**. These particles could be assigned to the dispersed NPs and more exfoliated layers of OMMT, which is also verified for C10A APTES MNCs, as shown in **Figure 5 (F)**. These results are in concordance with XRD that suggests a partial intercalation of APTES NPs in the layers of MMT.

Regarding the coating of APTES on Fe_3O_4 NPs, it is difficult observe changes in morphology for both types of magnetic nanoclays, Na116 and C10A. [41]

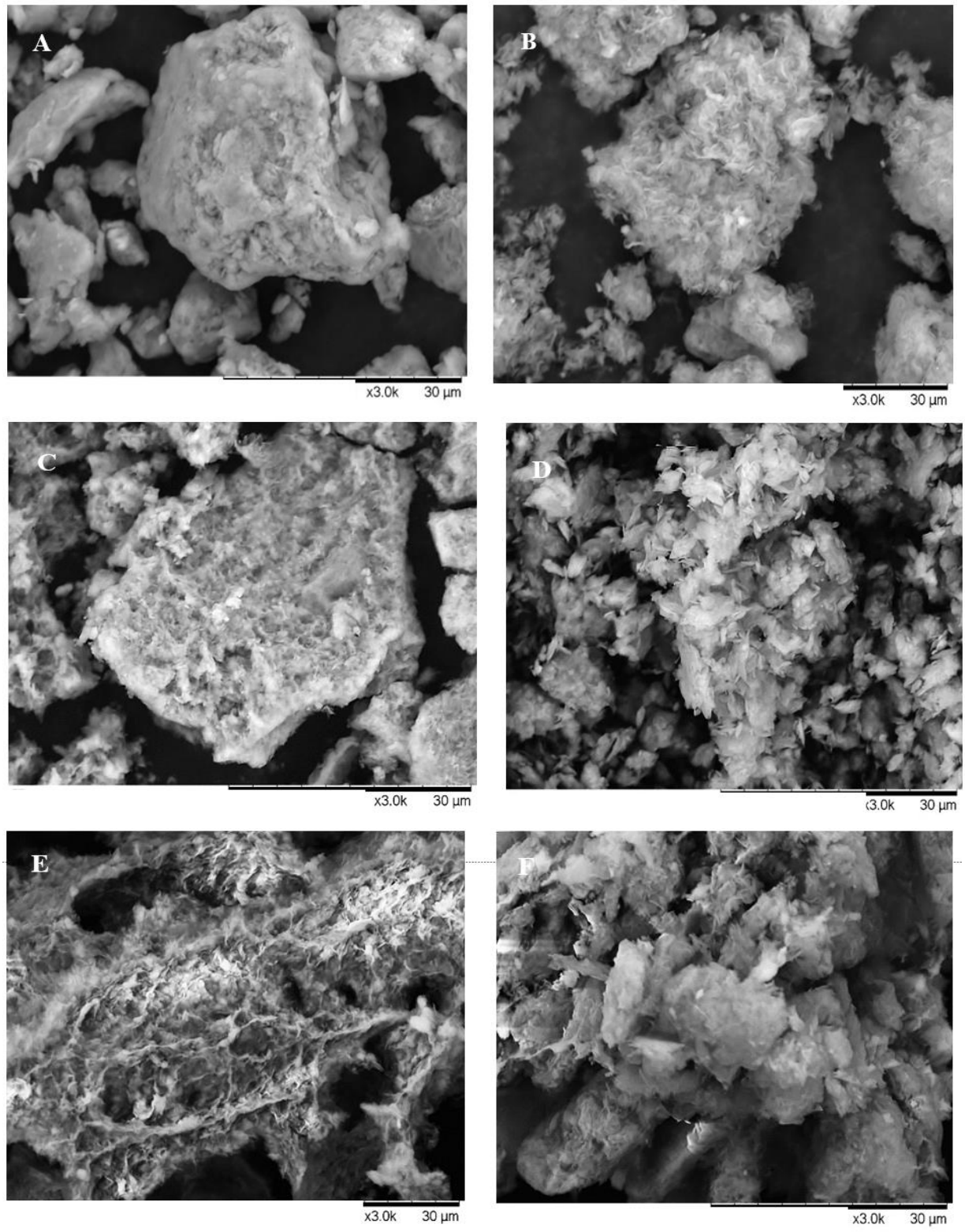

Figure 5 – **Scanning electron microscopy micrographs** of **(A)** pristine **MMT**, **(B) OMMT**, **(C) Na116 MNCs**, (**D) C10A MNCs**, **(E) Na116 APTES** and **(F) C10A APTES** MNCs.

Moreover, **Figure 6** and **Figure 7** shows the EDS color mapping for pristine MMT and OMMT, and Na116 MNCs, respectively. EDX was also performed to verify the surface composition of MMT, OMMT and MNCs before and after the modification. The primary components of MMT such as

silicon (Si), oxygen (O), carbon (C), aluminium (Al) and sodium (Na), were detected in all clay samples, as shown in **Figure 6**.

The weight percentage (**Table 1**) of O, C, Si, and Na components in MMT were 58.65%, 10.40%, 20.33% and 3.37%, respectively, whereas the OMMT shown weight percentage around 42.75%, 37.02%, 15.49% and 0.00%, respectively. Furthermore, the presence of Na is observed in **Figure 6** in the pristine Na^+ MMT and not in OMMT, as expected. After organophilization of MMT, the C peak appeared accompanied with the vanishing of Na peak. This suggests that most of the Na^+ cations on the clay surface have been exchanged by the alkylammonium cations, demonstrating the potential of organomodification. Additionally, the higher C content in OMMT when compared with pristine MMT, is due to the organic intercalant used in the OMMT. [60]

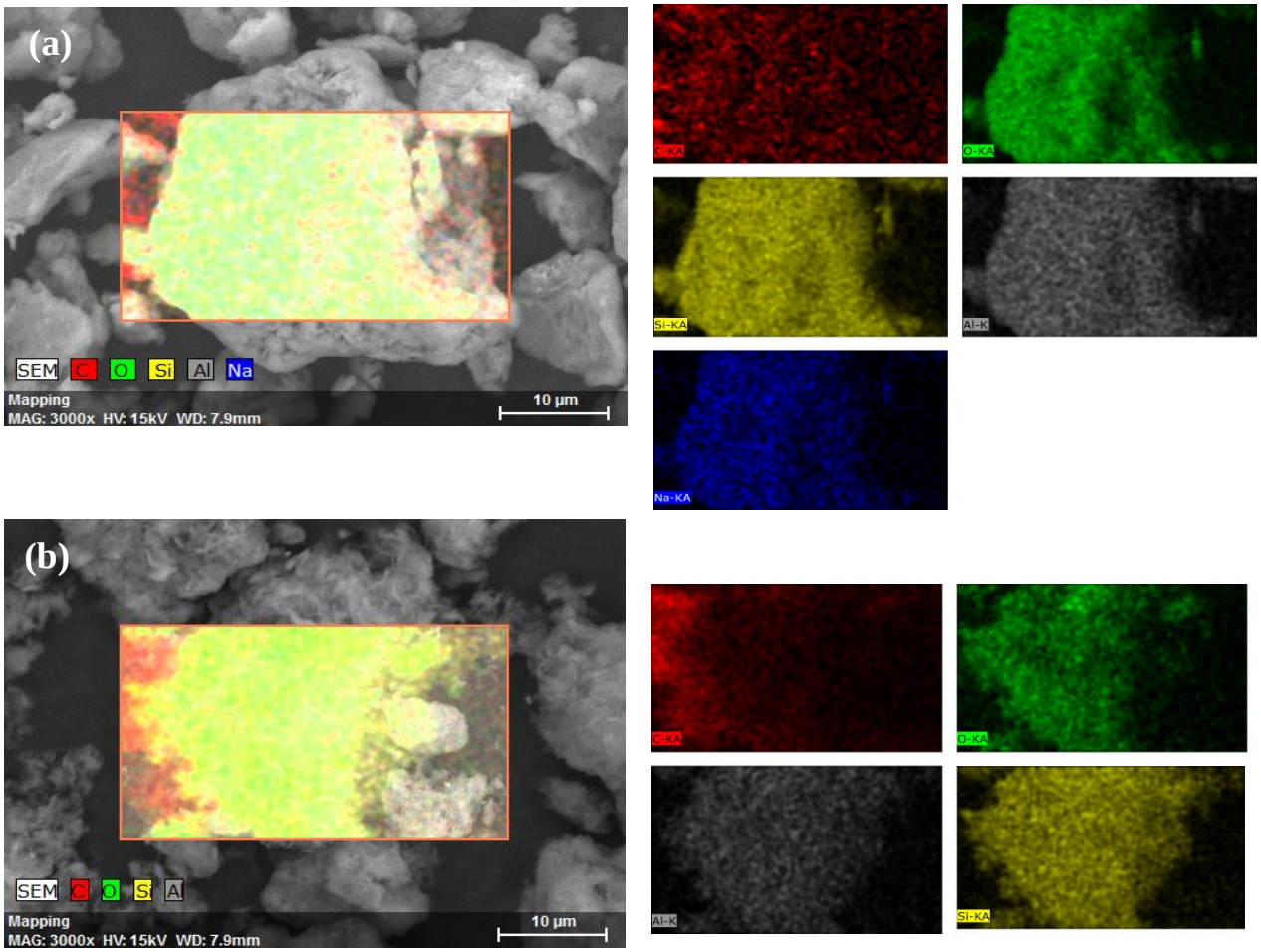

Figure 6 – **EDS mapping** of carbon, oxygen, silica, aluminium, and sodium for **MMT (a)** and **OMMT** clay **(b)**.

Table 1 - **Energy dispersive X-ray spectroscopy** components wt. % of **MMT and OMMT.**

C Atom. C [wt.%]		
Element	**MMT**	**OMMT**
O	58.65	43.75
C	10.40	37.02
Si	20.33	13.49
Na	3.37	0.00
Al	7.25	5.74
Total	100.00	100.00

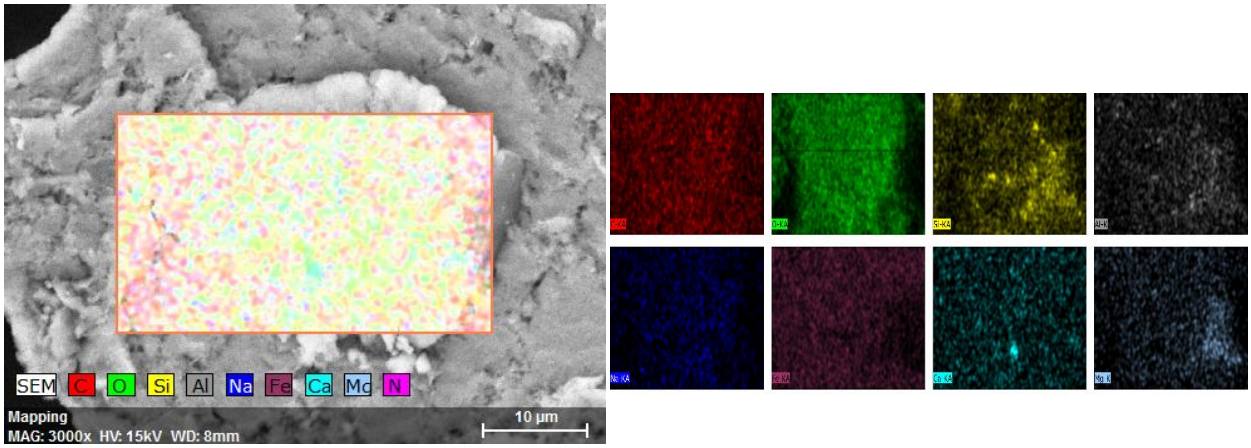

Figure 7 - **EDS mapping** of carbon, oxygen, silica, aluminium, sodium, iron, calcium, magnesium, and nitrogen for **Na116 MNCs**.

Figure 8 shows the EDX spectrum of Na116 MNCs in the presence of oxygen and iron peaks that reveal the existence of Fe_3O_4 NPs. In **Figure 8,** the peaks around 1.7, 2.7, 2.9, 3.7, 4.0, 4.5, 6.4 and 7.1 keV are related to the binding energies of MMT. The peaks around 0.7, 0.9, 6.4 and 7.0 keV are related to Fe_3O_4 NPs elements. Moreover, **Figure 9** indicates Na116 APTES MNCs with a very increased amount of C and Si, and the N peak appears more pronounced given by the APTES presence and composition. [41] [60]

Additionally, the EDX analysis of Na116 MNCs and Na116 APTES MNCs confirm the presence of elemental compounds in the MMT, which means the NPs were successfully intercalated or adsorbed to the surface of the nanoclays.

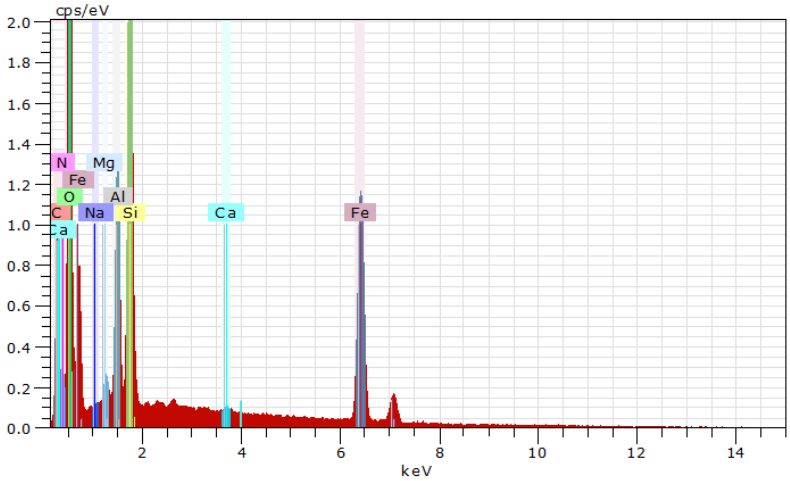

Figure 8 - **Energy dispersive X-ray spectroscopy** spectrum and elements of **Na116 MNCs.**

It should be noted that the EDX spectra for C10A clays is very similar to the others represented above. Therefore, the SEM EDS detailed data for all samples are shown in the **Appendix A.2.**

Concerning the C10A magnetic nanoclays, one should expect that the amount of nitrogen (N) in the C10A APTES MNCs would be higher than the ones without the APTES coated NPs, which is not verified by **Table 2**. These results suggest that the APTES Fe_3O_4 NPs were not successfully grafted on the layers of OMMT. Also, because of the high percentage of iron (Fe) in the C10A MNCs (20.01%) comparing to C10A APTES MNCs (4.69%), it proposes that only a reduced amount of NPs were intercalated and/or exfoliated in the clay layers of the latter.

Hence, the SEM EDS analysis confirmed that, from all magnetic nanoclays here described, the synthesis of Na116 and Na116 APTES MNCs seemed to be more efficient.

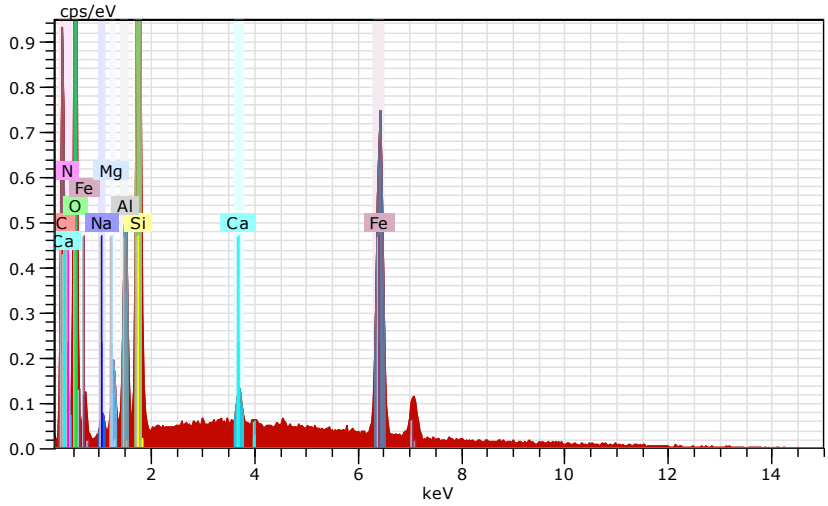

Figure 9 - **Energy dispersive X-ray spectroscopy** spectrum and elements of **Na116 APTES MNCs.**

Table 2 - **Energy dispersive X-ray spectroscopy** components wt. % of all **magnetic nanoclays.**

C Atom. C [wt.%]				
Element	**Na116 MNCs**	**Na116 APTES MNCs**	**C10A MNCs**	**C10A APTES MNCs**
O	46.25	30.55	43.45	33.23
C	19.75	28.76	18.88	42.63
Fe	29.80	16.38	20.01	4.69
N	0.00	1.71	2.26	1.08
Si	2.00	15.27	10.02	12.04
Al	0.78	4.65	4.20	5.31
Na	0.54	0.63	0.25	0.19
Mg	0.39	1.58	0.73	0.75
Ca	0.49	0.46	0.19	0.07
Total	100.00	100.00	100.00	100.00

ATR-FTIR provides the identification of the chemical groups presented in the samples of NPs or MNCs through the vibration modes characteristic of the chemical bonds, as different materials have a unique combination of atoms.

FTIR spectrum of naked Fe_3O_4 NPs, represented in **Figure 10 (A),** shows the presence of specific absorbance band at 560 cm^{-1} for this molecule which is attributed to the Fe–O bond and confirms the presence of an iron oxide core, while the band at 1590 cm^{-1} is related to the O-H and the band between 3000 cm^{-1} and 3500 cm^{-1} is related to the O-H stretching vibration mode due to water vapor. [5] [39]

The influence of the surface modification of SPIONs with APTES is also shown in **Figure 10 (A)** and the chemical bonds belong to the predominant functional group of the stabilizer. It is possible to identify a band at 1630 cm^{-1} which corresponds to the N-H bending mode of the free NH_2 group, while the absorbance band around 1100 cm^{-1} is the stretching vibration of Si-O. The characteristic adsorption

peaks of Fe-O band (at 560 cm^{-1}) shifted to slightly higher wavenumber, which also demonstrates that APTES was successfully chemically bonded to Fe_3O_4 NPs. [5] [40]

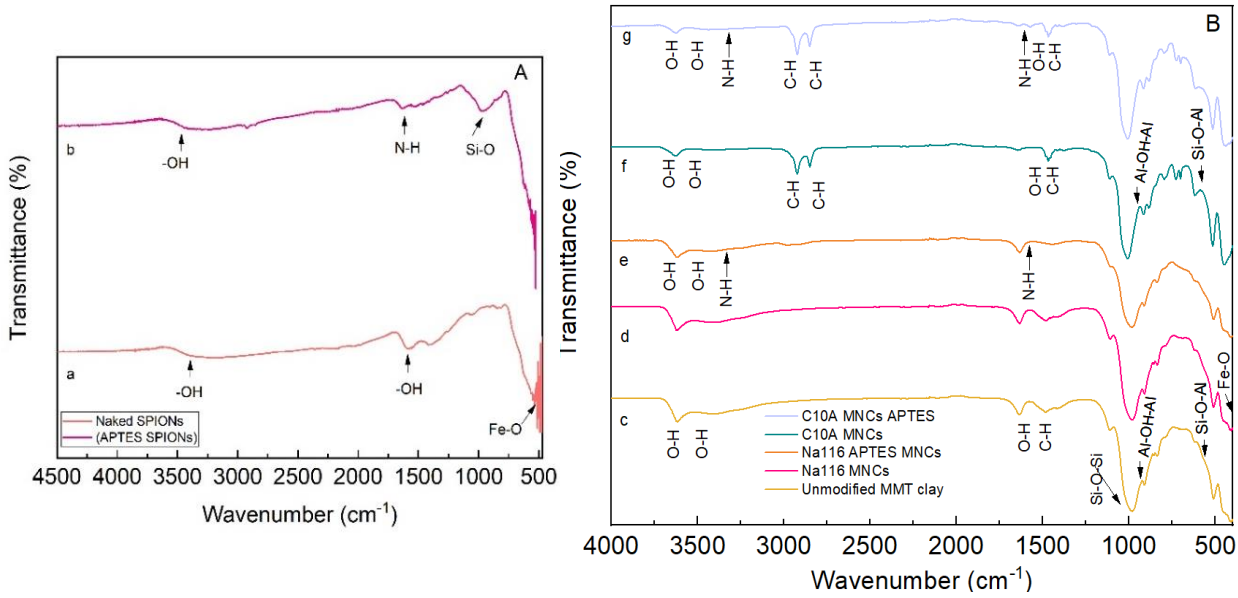

Figure 10 – **ATR-FTIR Spectra of iron oxide nanoparticles and magnetic nanoclays. A)** Naked Fe_3O_4 NPs (a), APTES coated NPs (b). **B)** unmodified MMT NA116 (c), NA116 MNCs (d), NA116 APTES MNCs (e), C10A MNCs (f), C10A APTES MNCs

Regarding the magnetic nanoclays, **Figure 10 (B),** shows the unmodified MMT revealing the bending mode of Al-OH-Al at 910 cm^{-1} due to the large amount of Al in the octahedral site of oxygen and the characteristic absorption bands near 3619 cm^{-1} (which is indicative of the presence of MMT in bentonite) due to –OH stretching mode of interlayer water. The overlaid absorption band in the region of 1640 cm^{-1} is assigned to the –OH bending mode of adsorbed water and the region of 1485 cm^{-1} to the C-H bending. These data indicate that some water molecules were entrapped in MMT. The characteristic band around 1110 cm^{-1} is due to the Si–O–Si stretching vibration for layered silicates and the band around 510 cm^{-1} is assigned to the Si–O–Al bending mode. [57]

However, the appearance of some bands in organically modified nanoclays' spectra (C10A MNCs) that are not shown in the pristine MMT, located at 2922 and 2851 cm^{-1}, are attributed to the stretching of C-H methyl and methylene groups from the organic modifier chemical structure. The bands corresponding to adsorbed water (3619 cm^{-1} and 1640cm^{-1}) are clearly less visible in the C10A MNCs spectra than in the pristine MMT, which may be due to the hydrophobic characteristics of these type of clays. Na116 MNCs' surface has a more hydrophilic character than C10A MNCs since the incorporation of an organic modifier improves the hydrophobicity of clays. Despite the differences in the organic modifier C10A, their functional groups are very similar. Although the C10A MNC has a benzyl group in the organic modifier, its presence could not be verified by this FTIR analysis.

Figure 10 B (d)-(g) show that there were not significant changes in the spectra of MNCs compared to unmodified MMT showing the same characteristic bands. Compared to the bonds in pristine MMT, most bonds in MNCs and APTES MNCs are in the same positions, and this means that their basic chemical structure remain unchanged after loading Fe_3O_4 NPs or APTES NPs. However, the successful modification of magnetic clays' surface with APTES coating is more easily confirmed by **Figure 10 B (e), (g)** because APTES show the characteristic bands at 1630 cm^{-1} corresponding to $–NH_2$ bending vibration of modifier molecule, as mentioned before. However, it is a small band due to the small concentration of APTES in the magnetic clays. [35]

These results are coherent with XRD analysis indicating that only with an increased percentage of NPs in the magnetic clays a better intercalation could be verified. Thus, because of van der Waals interactions between the oxygen groups of MMT and NPs, peaks would probably shift to lower wavenumbers and the bands intensity would decrease. [40] [41]

Despite, XRD and FTIR analysis may reveal if clay modification with NPs occurred, for better understanding the physical and chemical changes is better to complement this with some other techniques, such as thermogravimetric analysis. This results on a weight loss as a function of temperature graph which gives more insight into the quantity of organic modifiers present in the magnetic clays and their thermal stability.

TGA curves for Fe_3O_4 SPIONs and APTES SPIONs are displayed in **Figure 11 (A)**.

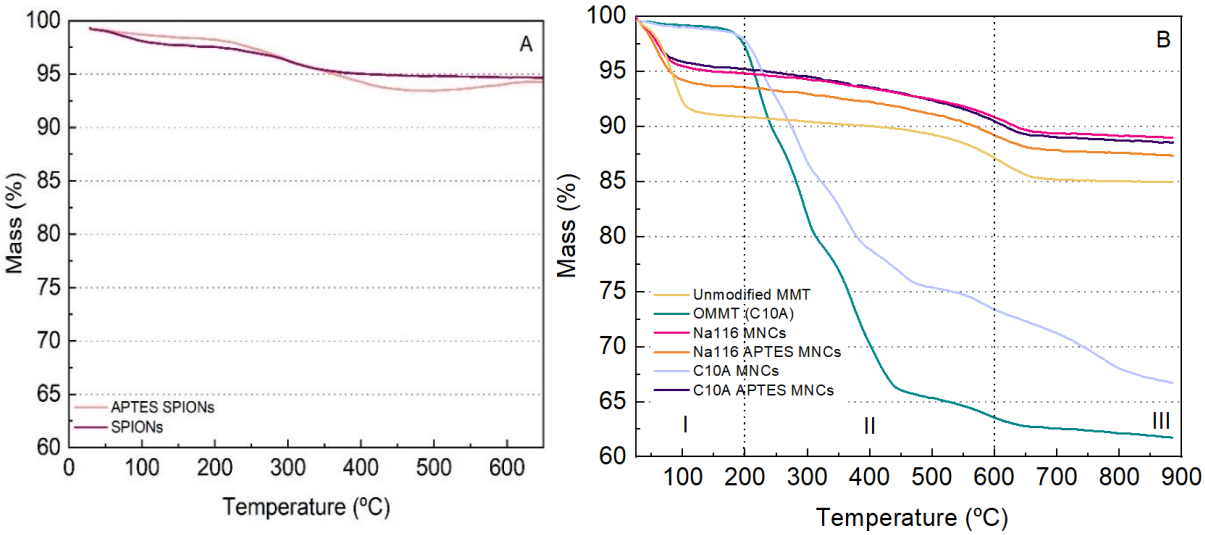

Figure 11 – **TGA curves for: A)** naked SPIONs, APTES SPIONs and **B)** MMT, OMMT and all magnetic nanoclays.

As expected, Fe_3O_4 NPs are not degraded in the tested range. The small reduction in weight loss is related to the conversion of magnetite to maghemite, which are the stable phases of diagram of Fe-O system above 570 ºC. [35]

Nevertheless, when Fe_3O_4 SPIONs are stabilized with surfactant typical degradation stages of those molecules appear in the TGA curves. Thus, the decomposition of the organic ligand is characterized by a first step above 200 ºC, attributed to the evaporation of the surface adsorbed water and a second one in the 500-800 ºC range due to the decomposition of APTES coating and the condensation of OH groups of silanols (Si-OH), as previously reported in literature. [42] Therefore, APTES NPs present a higher temperature variation. For this sample the total weight loss is approximately 6.43%.

Figure 11 (B) shows the TGA curves of the MMT, OMMT and its derivates. The first region (I) of the TGA curves, up to 200º C, is attributed to the evaporation of adsorbed water (desorption of water molecules from MMT layers). When comparing pristine MMT with OMMT, the first weight loss is higher due to the displacement of interlayer water in organic modified MMT and increasing hydrophobicity after organophilization.

The second region (II) takes place between 200º C and 600º C and the weight losses are assigned to decomposition of adsorbed or chemically grafted modifiers from the surface of organic modified MMT or materials between layers which confirms the intercalation. [43] Thus, based on the percentage of lost weight between 200ºC and 600ºC, it is possible to calculate the quantity of grafted or adsorbed modifier on the clay surfaces.

Lastly, the weight loss above 600º (III) corresponds to the shrinkage of hydroxyl groups of structural aluminosilicates after surface modification, showing an increased weight loss for organic modified MMT compared to pristine MMT, validating the potential of organophilization. [13] [15]

Consequently, **Figure 11 (B)** indicates an abrupt mass drop below 200 ºC for unmodified MMT and Na116 MNCs meaning a considerable higher amount of water adsorbed by those samples, proving that this type of clay is the one with higher hydrophilic character compared with the organic modified C10A MNCs, as predicted. The entanglement of water molecules within the clay structure due to constraint caused by intercalated NPs' molecules, might also shift the water evaporation to higher temperatures. Thus, as SPIONs are added the amount of water in Na116 clays is expected to decrease and to increase in C10A clays.

In addition, the weight loss of Na116 MNCs and Na116 APTES MNCs at 200–600 ºC is attributed to desorption of crystal water, indicating that some of the crystalline water molecules in the clays layer are exchanged with other ions. Above 600 ºC occurs the decomposition of Fe_3O_4 and APTES NPs. In the temperature range from 600 to 900 ºC, the weight change of unmodified MMT, Na116 MNCs and Na116 APTES MNCs is caused by the decomposition of structural hydroxyl groups. [37] Therefore, Na116 clays in the presence of APTES NPs have less temperature variation compared to MMT and it degrades more than Na116 MNCs, since Fe_3O_4 NPs do not degrade with temperature in the tested range. Regarding the C10A MNCs and OMMT the same behaviour is observed. The OMMT decomposition rate changed from a drastic weight loss to a slower and more gradual one in C10A MNCs, owing to the presence of SPIONs.

Although, the outcome for C10A MNCs and C10A APTES MNCs were unexpected. As the encapsulation of NPs in clays is improbable to happen only for APTES SPIONs, the most likely assumption would be that the presence of APTES molecules forced the organic modifiers to leave C10A, remaining only a small quantity of Fe_3O_4 SPIONs. This would explain the unusual similarity of C10A APTES MNCs pattern with unmodified MMT. In the case of C10A MNCs without any stabilizing agent, the opposite would have happened leaving only residues of SPIONs that can lead to further degradation with temperature. These results agree with the SEM EDS analysis confirming that the encapsulation of APTES NPs in the C10A clays was low.

Table 3 summarizes the thermogravimetric analysis showing the water content (which is calculated as the mass loss at 200 ºC), the content of organic modifier in each clay (given by the mass loss between 200 and 900 ºC) and the total weight loss given by the total amount of these two. In general, it can be considered that the residual mass is the inorganic material that remained. [44]

Table 3 - **Data from TGA-DSC** analysis characterization for all nanoclays.

Clay	Water content (wt.%)	Modifier content (wt.%)	Total weight loss (%)
Na116 (MMT - Unmodified MMT)	8.80	5.98	14.78
C10A (OMMT - Organic modified MMT)	2.40	35.60	38.00
Na116 MNCs	4.41	6.68	11.09
Na116 APTES MNCs	6.25	6.23	12.48
C10A MNCs	6.39	32.41	38.80
C10A APTES MNCs	4.88	5.92	10.80

Considering the data from **Table 3**, it can be said that in certain way the intercalation of NPs in clays was achieved and their thermal stability improved as well. Thus, it is possible to conclude that Na116 MNCs possess excellent thermal stability since it practically does not degrade with temperature (11% total weight loss), whereas MMT exhibited poor thermal stability, losing almost 15.0% of its mass associated with adsorbed water and hydroxyl groups. This evidence is in concordance with the literature. [37]

3.2. Magnetic Hyperthermia

Magnetic hyperthermia assays were performed to evaluate the heating capacity of NPs into the magnetic clays. The study was conducted using previously prepared clays which includes incorporated iron oxide NPs in the solution. Since 20% (w/w) of NPs were incorporated into clay solutions, tests were carried out at concentrations of 2.5 mg mL^{-1}. This way, it is possible to compare the heating capacity since all components have the same theoretical concentration of NPs. Three tests for each sample were analysed to have a better statistical analysis. They were analysed for 10 minutes, with a magnetic flux density of 300 Gauss and a frequency of 388.40 kHz. **Figure 12** shows the temperature variations of both types of NPs and all magnetic nanoclays.

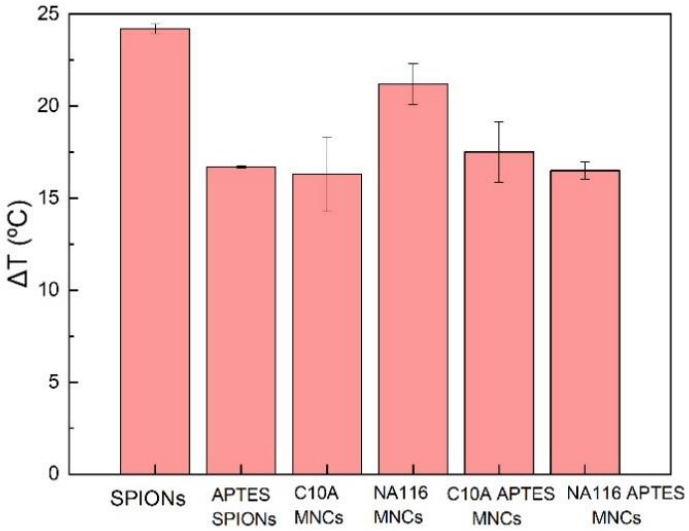

Figure 12 - **Temperature variation of naked SPIONs, APTES coated SPIONs and all MNCs** 2.5 mg mL^{-1}. Assays were carried out for 10 minutes at a magnetic flux density of 300 Gauss. The results are expressed as average ± standard deviation for 3 independent experiments.

To recognise the efficiency of NPs there is a need to calculate the specific absorption rate (SAR). This indicates the rate of heat evolution in hyperthermia through the efficiency of the magnetic NPs to convert an alternating magnetic field into heat. This phenomenon happens due to two types of relaxation: Brownian and Néel [45]. When Fe_3O_4 NPs are in suspension, Brownian and Néel relaxations are present. Brownian relaxation mechanism is dominant involving the rotation of the particle itself against the forces coming from the solution while Neéls' relaxation comes from to the rotation of the particles' magnetic moment to the equilibrium state without implying the rotation of the particle. When they are under the effect of an alternating magnetic field it provides energy to the magnetic moments of the particle so that they can get out of their equilibrium state and the energy begins to be dissipated. [29]

Comparing the temperature difference of naked SPIONs and APTES coated SPIONs, it is possible to acknowledge that APTES SPIONs presents an inferior temperature difference for the same iron concentration. These results reveal that naked SPIONs are those with the greatest temperature variation (24.2ºC) and consequently, with the highest SAR value (16.6 W g^{-1}) as illustrated in **Figure 12** and **13**, respectively.

Regarding the behaviour of NPs coated with APTES there is a slight decrease in temperature **(**16.7°C) and SAR (11.8º $W.g^{-1}$). One possible explanation for this might be the shielding effect of the alkyl silane layer, being expected due to the presence of the two relaxations already mentioned. [29] [46]

When aggregates are present these NPs see their mobility, magnetization and heat ability diminished as they behave like ferromagnetic particles not being capable of fully align their anisotropic

axis with the magnetic field. [47] Hence, the presence of APTES coating on Fe_3O_4 NPs significantly influence their generated temperature as can be seen from the 7.5º C variation between them. Also, it is noticeable the higher temperature variation (21.2ºC) and SAR (14.3 $W.g^{-1}$) for NPs encapsulated into pristine MMT (Na116 MNCs) compared with APTES Na116 and C10A MNCs (11.6 $W.g^{-1}$ and 10.6 $W.g^{-1}$, respectively). This may be because the stabilizing agent forms a layer around the nanoparticles, acting as a heat sink, which can decrease their magnetic properties restricting their ability to generate heat. Moreover, as C10A clays have hydrophobic properties, a possible reason is the entrapping of NPs into the clays in such a way that Brownian relaxation is reduced. [29]

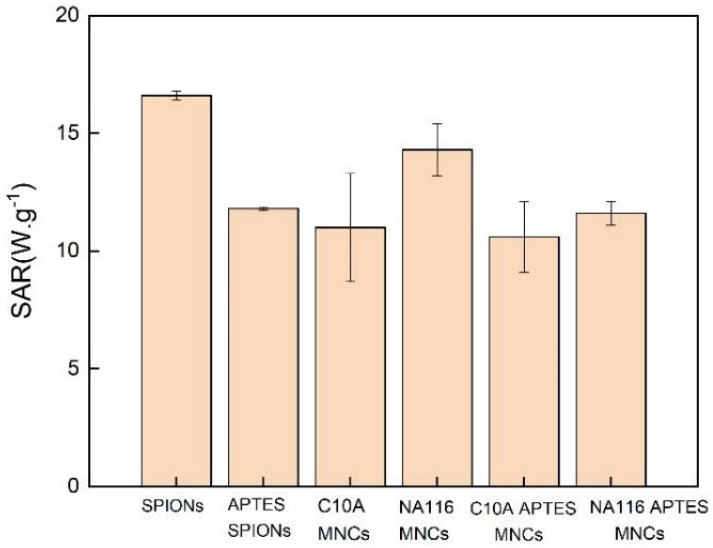

Figure 13 – **Comparison of the SAR values** of pristine NPs, APTES NPs and all magnetic nanoclays. The results are expressed as average ± standard deviation for three independent experiments.

For all components, the temperature difference for the same concentrations is not very different which can be an indicator of the good incorporation of the NPs in the magnetic nanoclays produced.

The NPs to be used in the treatment for magnetic hyperthermia need to reach a temperature around 42.5 °C, in which the tumour cells enter apoptosis. Considering that the human body is, on average, at 37 °C it is necessary to obtain a variation of approximately 5 °C. Thus, all MNCs are very close to the variation that is supposed to be obtained, so it is concluded that a concentration of 2.5 mg mL^{-1} might be sufficient to generate the required temperature for magnetic hyperthermia studies. Even though, from all the suspensions the one that possess the greatest heating capacity is concluded to be Na116 MNCs. The results agree with the previous TGA analysis that showed that these type of magnetic nanoclays could support high temperatures.

To improve further studies, it would be probably necessary to test other times under the effect of a magnetic field or the concentration of NPs to obtain a greater efficiency in terms of temperature variation.

3.3. Enzymatic assays

3.3.1. Nanozyme activity (U) and specific activity (SA)

According to the definition of the Nomenclature Committee of the International Union of Biochemistry, "one unit (U) of enzyme catalyses the transformation of one micromole of substrate per minute under their recommended standard conditions". [49] Catalytic activity expresses "the rate of the catalysed conversion of a specified chemical reaction produced in a specified assay system" and specific

activity (SA) is the enzyme activity per milligram (U mg^{-1}). U catalyses the conversion of 1 micromole of substrate per minute.

The nanozyme activity (U) and specific activity (SA) is calculated based on the following equations:

$$\text{Nanozyme activity } (\mathbf{U}) = \frac{\mathrm{V}}{(\varepsilon \times l)} \times \left(\frac{\Delta \mathrm{A}}{\Delta \mathrm{t}}\right) \qquad \textbf{Equation 5}$$

where **V** is the total volume of solution (μL); **ε** is the molar absorptivity (39,000 M^{-1} cm^{-1} for TMB and 43.6 M^{-1} cm^{-1} for H_2O_2, at 562 nm and 240 nm, respectively); $\boldsymbol{l}$ is the optical path length (cm) and $\boldsymbol{\Delta A/\Delta t}$ is the change in absorbance per time unit at initial rate conditions, where a linear dependence of A vs. t is expected. [49]

$$\text{Specific activity } (\mathbf{SA}) = \frac{U}{m} \qquad \textbf{Equation 6}$$

where $\boldsymbol{m}$ is the nanozyme amount (mg).

3.3.2. Catalytic activity of NPs and magnetic nanoclays

One of the main purposes of this work is to study the enzymatic-like activity of the MNCs produced. It is crucial to learn how surface coatings influence the catalytic activity of magnetic nanoclays since coatings are often used to offer stability to the NPs by preventing their aggregation and loss of magnetic properties. Although, it is expected that some modifications may occur due to the thickness, functional groups, and surface charge of coating, which can either enhance or hamper peroxidase and catalase-like activities. [50] The latter depend on pH and, therefore, this parameter was also considered in the assays performed.

Another assessed parameter was MNCs stability after a week and a month of storage through the retained activities. All the results of the specific activities are presented in **Tables 5, 6 and 7**.

3.3.2.1. Peroxidase-like activity assays

As a first approach, it was important to understand if SPIONs had indeed the enzymatic-like activity, as previously reported. To do so, some visual tests were performed. The substrate used (TMB) has two amine groups and so it is more likely to have a stronger affinity toward a negatively charged NP surface. For peroxidase-like activity, the MNPs must first form a complex with their substrate before catalysis can occur. [51] However, the APTES coating is cationic due to its amine group, and this can hamper peroxidase-like activity compared to other coatings.

NPs require a pH value between 3.5 and 6 to have a significant peroxidase-like activity and to be relevant in the cellular environment as these pH levels are only found in lysosomes (pH 5.5). [52] As demonstrated by Chen *et al* and Gao *et al* [22] [54], the optimal pH is 3.5 for APTES coated NPs and do not exhibit peroxidase-like activity under neutral pH conditions. Therefore, in this work it was confirmed the preponderant peroxidase-like activity for a pH 3.5. However, in a future application it would be essential to study a pH closer to the physiological one.

As TMB acts as a hydrogen donor for the reduction of H_2O_2, this will cause an immediate color change to blue in the reaction system. [17] **Figure 14** shows the colorimetric effect of the surface coating for peroxidase-like activity at pH 3.5 for APTES coated SPIONs, as well as Na116 MNCs and APTES coated Na116 MNCs.

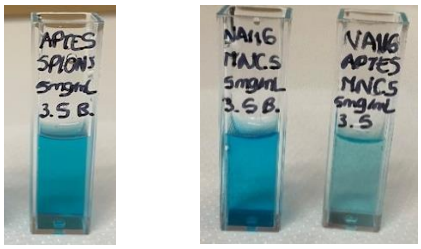

(A) **(B)**

Figure 14 – **(A) Colorimetric assay using TMB as substrate for APTES NPs** (1870 µL of 100 mM buffer pH 3.5; 100 µL of 10 mg mL^{-1} TMB; 5 µL of 5 mg mL^{-1} APTES coated SPIONs, 25 µL of 8.8 M H_2O_2) and **(B) Na116 MNCs** (1865 µL of 100 mM buffer pH 3.5; 100 µL of 10 mg mL^{-1} TMB; 10 µL of 5 mg mL^{-1} MNCs; 25 µL of 8.8 M H_2O_2), naked (left) or coated with APTES (right).

It is clear that all NPs tested exhibited peroxidase-like activity under acidic pH. In terms of coloration, all cuvettes present a similar intensity so it should be expected a similar behaviour in terms of absorbance. Experimental conditions were selected to keep absorbance values below 1, as readings above this value might not be accurate. [53]

3.3.2.2. Catalase-like activity assays

Firstly, was important to see if it was possible to measure the catalytic activity at a wavelength of 240 nm. As seen in **Figure 15**, the NPs do not present a peak at this wavelength. Hence, it was confirmed that the catalase-like activity of NPs and, consequently, magnetic nanoclays can be measured through H_2O_2 decomposition at 240 nm. Absorbance measurements at this wavelength were conducted in quartz cuvettes.

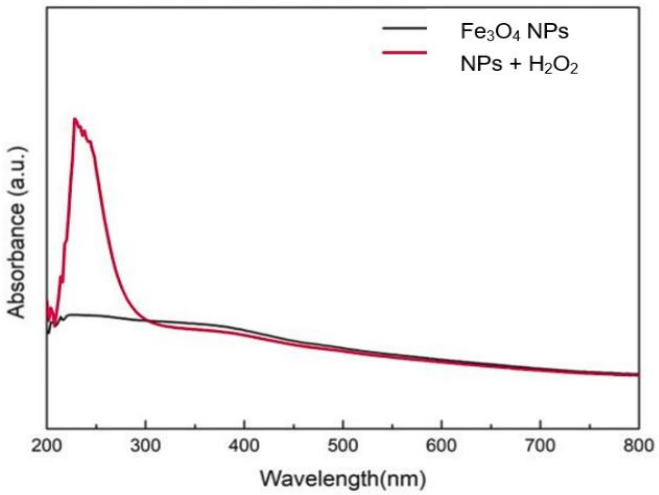

Figure 15 - **Absorbance spectrum of hydrogen peroxide and NPs.** This assay was carried out using 10 µL of 5 mg mL^{-1} APTES SPIONs and 20 µL of H_2O_2 0.88 M, in 1mL of phosphate buffer (100 mM, pH 6.0).

One of the first tests made to assess if there was any catalase-like activity of SPIONs and MNCs is represented in **Figure 16 (A).** By adding a small quantity of NPs and H_2O_2 to the cuvette it was immediately observed a considerable amount of gas bubbles due to oxygen formation. Also, it was necessary to evaluate if these bubbles affected the measurement, which they did not. According to Chen *et al.* and Gao *et al.,* [22] [54] the IONzymes possess catalase-like activity under neutral and basic pH conditions, it being non-existent at acidic pH and having its peak at pH 7.4.

Therefore, catalase-like activity assays were conducted at pH 6 and 7.4 as a reference but also to better mimic the intracellular environment of the cytosol. At this pH values peroxidase-like activity is almost inexistent, as already mentioned.

(A) 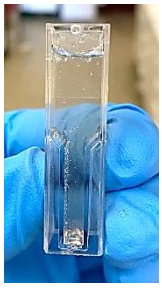  **(B)**

Figure 16 – **Assays to assess the catalase-like activity of APTES SPIONs. (A)** 5 µL of APTES SPIONs 5 mg mL^{-1}, 1 mL of phosphate buffer (10 mM, pH 7.4) and 20 µL of 0.88 M H_2O_2. **(B)** Assay carried out using 10 µL of APTES SPIONs 5 mg mL^{-1} and 20 µL of 0.88 M H_2O_2, in 1 mL of phosphate buffer (10 mM, pH 7.4), in a quartz cuvette.

Then, it was crucial to understand how much time it takes to measure the catalase-like activity. Following a protocol from Mu *et al.* [55] where another type of MNPs were used, it was possible to reproduce the conditions of the assay since it takes a certain time to see considerable changes in absorbance. Therefore, the assays were conducted for 5 minutes.

It should be noted that the readings during the first seconds of experiment were discarded due to the instability caused by magnetic nanoclays in suspension. Also, and given the differences in MNCs, preliminary tests were made to optimize the amount of each type of MNC introduced in the quartz cuvette, **Figure 16 (B)**. It was concluded that this amount should be a reasonable quantity, because very low amounts of MNCs did not produce significant changes in absorbance, and high amounts of MNCs caused saturation. Optimized values of the amounts of MNCs used are given in the table below. These parameters are maintained for both pH 6 and pH 7.4.

Table 4 - **Optimized values and quantities used for the buffers**, **MNCs and H_2O_2 for catalase-like activity assays.** Assays were carried out using 5 mg mL^{-1} of the different types of nanoparticle suspensions, 1 mL of phosphate buffer (10 mM pH 7.4 or 10 mM pH 6.0), and 20 µl of 0.88 M H_2O_2.

APTES SPIONs	NA116 MNCs	NA116 APTES MNCs	C10A MNCs	C10A APTES MNCs
10 µl APTES NPs	50 µl of MNCs	50 µl of MNCs	80 µl of MNCs	80 µl of MNCs

3.3.2.3. Effect of the surface coating for peroxidase-like and catalase-like activities and specific activities

The specific activity results for peroxidase-like activity (sodium acetate buffer pH 3.5, 100 mM) and catalase-like activity (phosphate buffer pH 6 and pH 7.4, 10 mM) of APTES coated SPIONs and all magnetic nanoclays, freshly produced, are shown in **Tables 5, 6** and **7,** respectively.

The S_A values shown on the tables are averages of results obtained from different assays, converted to enzyme activity per milligram (**Equation 5**).

Figure 17 shows some of the results obtained for peroxidase-like activity assays performed with magnetic nanoclays. Those for APTES SPIONS are given both on the left and on the right figures, for comparison. When observing the graphs, it is possible to acknowledge that in terms of absorbance there is a clear difference between APTES NPs and MNCs. Naked SPIONS are not stable in an aqueous suspension and, thus, the effect of APTES coating on SPIONS could not be assessed. In the case of the MNCs, the figures suggest that the APTES coating has a negative effect, since its presence decreases the slopes of the lines. The assays with APTES coated MNCs were carried out with a larger amount of material. When this is considered and specific activities are calculated, the APTES coating is seen to hamper the peroxidase-like activity, which can be explained by the low affinity of TMB towards a cationic coating.

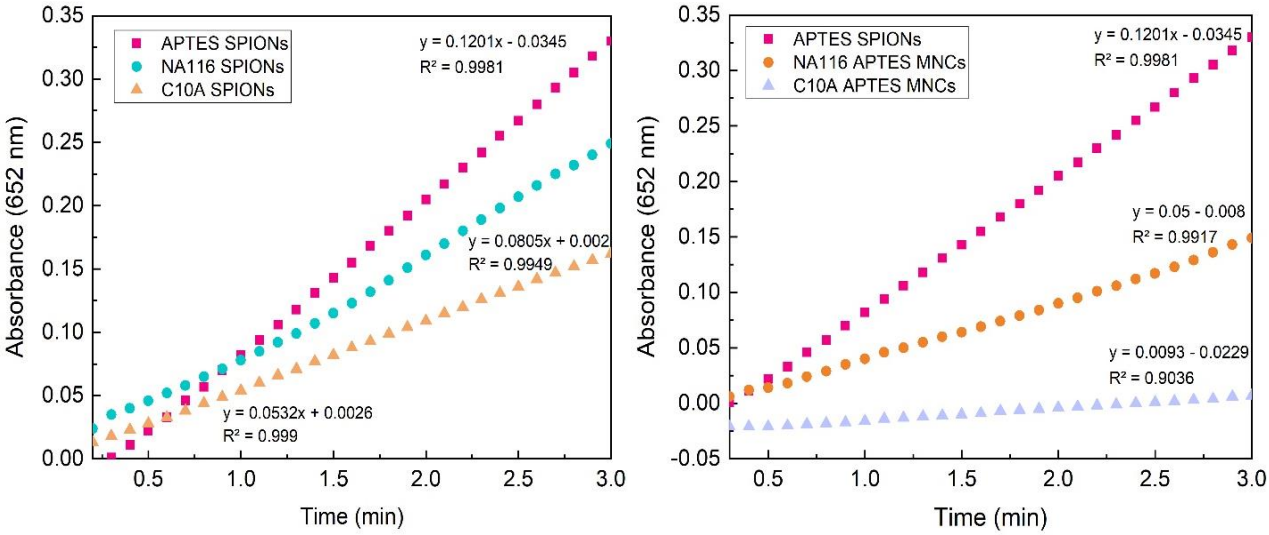

Figure 17 - **Effect of surface coatings on peroxidase-like activity of MNCs.** 5 µL **APTES SPIONs** 5 mg mL^{-1}; 1870 µL sodium acetate buffer (100 mM, pH 3.5); 100 µL 10 mg mL^{-1} TMB; 25 µL H_2O_2 (8.8 M).
10 µL **MNCs** 5 mg mL^{-1}; 1865 µL Sodium acetate buffer (100 mM, pH 3.5); 100 µL 10 mg mL^{-1} TMB; 25 µL H_2O_2 (8.8 M). The assays were made in duplicate.

Table 5 - **Specific peroxidase-like activity values** of APTES coated SPIONs and all magnetic nanoclays at **pH 3.5.**

Specific activity (U mg^{-1})	**APTES SPIONs**	**NA116 MNCs**	**NA116 APTES MNCs**	**C10A MNCs**	**C10A APTES MNCs**
First assay	0.4 ± 0.1 (100%)	0.10 ± 0.02	0.09 ± 0.02	0.14 ± 0.03	0.12 ± 0.01
1 week after	0.32 ± 0.04 (81%)	0.088 ± 0.004 (86%)	0.08 ± 0.03 (93%)	0.088 ± 0.003 (62%)	0.061 ± 0.009 (53%)
1 month after	0.23 ± 0.02 (58%)	0.083 ± 0.001 (81%)	0.054 ± 0.003 (62%)	0.050 ± 0.007 (35%)	0.009 ± 0.001 (8%)

Another parameter assessed was the stability of the activity during the time of storage. The stability of the NPs tested decreases over time, as measured by the retention of catalytic activity. The obtained results suggest that APTES coating does not have a stabilizing effect, the loss of activity being more pronounced when an APTES coating exists. Besides this, the exchangeable cations on Na116 clays have a much stronger affinity to water molecules (positive charges) and thus provide a dominant force, contributing, as well, for this phenomenon. The almost complete loss of activity of C10A APTES MNCs after a one-month storage may be due to the oxidation of the NPs since their ideal storage validity is 2-4 weeks in aqueous suspension, adding to the surface coating of APTES contribution. Also, this type of clay and its organic modifier increases hydrophobicity and causes an agglomeration of clay platelets into larger particles. Since the properties of nanomaterials are size dependent and APTES is a larger molecule than naked NPs, the hydrodynamic diameter of APTES NPs is higher, reducing its peroxidase-like activity (smaller particles exhibit more activity). [56]

Nevertheless, it was expectable that after a month the peroxidase-like activity would be reduced, however still present. These results prove that all suspensions still possess some catalytic activity at an acidic pH being sufficiently stable in aqueous media (considering that the results for C10A APTES MNCs after 1-month storage are due to NPs oxidation).

The S_A of APTES SPIONS are higher than those of the MNCs. Of these, Na116 MNCs combine higher stability with the highest specific peroxidase-like activity.

Figure 18 shows some of the results that have contributed to the average catalase-like specific activity values given in **Table 6** and **7**. Again, results for APTES SPIONs are given both on the left and right figures, for comparison. Both at pH 6 and pH 7.4 naked SPIONs do not present any catalytic activity. Their inability to decompose the hydrogen peroxide is explained due to the lack of a surface coating, as without it the NPs are not stable in an aqueous suspension. Therefore, the effect of the APTES coating on SPIONS could not be assessed. **Figure 18** shows that APTES SPIONs and MNCs indeed possess catalase-like activity at pH 7.4.

Table 6 shows that the presence of APTES coating has little effect on the catalase-like activity of MNCs, freshly produced or after being stored for one week. After 1-month storage, APTES coating seems to have a stabilizing effect, especially in the case of C10A MNCs. This is expected due to the APTES coated SPIONs ability to decompose hydrogen peroxide compared with naked NPs.

In general, the values obtained after 1 week storage are lower than expected, since the trend seems to be high stability of the NPs up until one month of storage. Such lower activity values might be the result of a systematic error caused using an incorrectly calibrated micropipette. Although, there was a loss of replicas of the conducted assays after one month for both pH, which compromised further analysis.

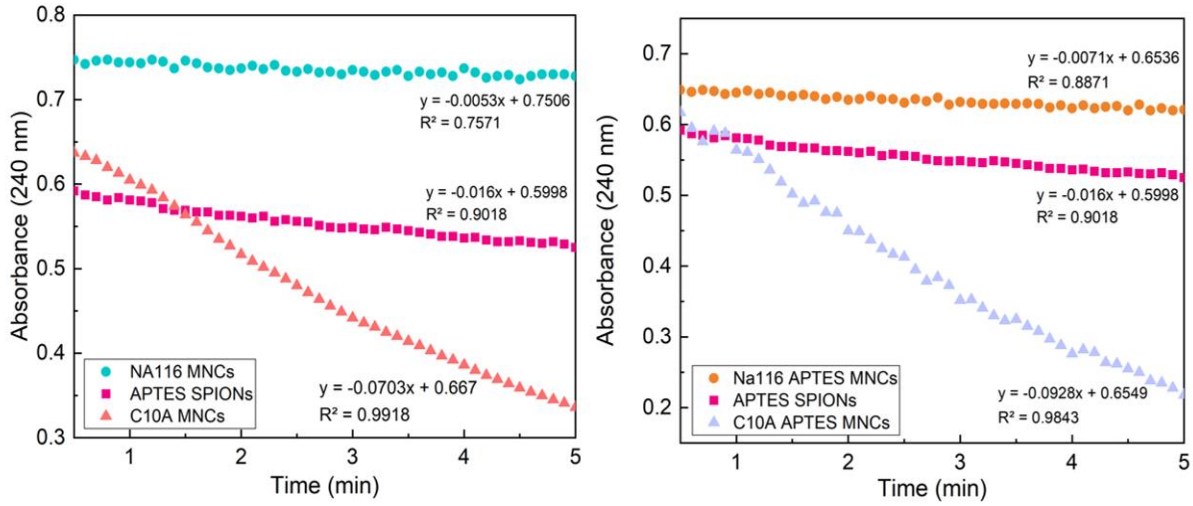

Figure 18 - **Effect of surface coatings on catalase-like activity of MNCs pH 7.4.** This assay was carried out using a specific quantity of 5 mg mL^{-1} APTES or MNCs, 20 µL of H_2O_2 0.88 M, in 1mL of phosphate buffer (10 mM, pH 7.4). The assays were made in duplicate.

Table 6 - **Specific catalase-like activity values** of APTES coated SPIONs and all magnetic nanoclays at **pH 7.4.**

Specific activity (U mg^{-1})	**APTES SPIONs**	**NA116 MNCs**	**NA116 APTES MNCs**	**C10A MNCs**	**C10A APTES MNCs**
First assay	9.0 ± 0.1 (100%)	1.2 ± 0.2	1.2 ± 0.8	7.8 ± 0.7	6 ± 1
1 week after	7 ± 1 (82%)	0.5 ± 0.2 (40%)	0.6 ± 0.2 (48%)	5.0 ± 0.4 (64%)	5.7 ± 0.5 (89%)
1 month after	9.0 (100%)	1.0 (83%)	1.2 (100%)	5.7 (73%)	7.2

The results for catalase-like activity assays at pH 6 are given in Figure **19** and Table **6**. The effect of the surface coating on catalase-like activity is shown in **Figure 19**. It is possible to certify that the catalytic activity also exists at pH 6.

As shown in **Table 7**, in this case, the presence of an APTES coating improves the catalase-like activity of NA116 MNCs but has the opposite effect on C10A MNCs. This was already apparent in **Table 6**, but less pronounced. Lower catalytic activity of C10A APTES MNCs relative to C10A MNCs

might be due to the hydrophobic properties of the organic modifier hampering the catalytic activity. Thus, even though APTES molecules are intercalated into C10A interlayers, this duality in nature might cause a decrease of catalytic activity.

Over a period of one month, all NPs except APTES SPIONS show a decrease in specific catalase-like activity. This loss of activity may be a consequence of the oxidation of the NPs, mentioned earlier. An agglomeration of clay platelets into larger particles can have a negative influence on catalytic activity. The activity values measured after a 1-week storage are either similar, or lower, than the values for the freshly produced NPs, and so the trend observed at pH 7.4, which might be due to a systematic error, is not observed.

The errors associated with the catalytic activity values measured are high. The MNCs suspensions must be well shaken before pipetting the amounts required for reaction. More assays should have been performed at the same experimental conditions. Even so, the results suggest that the MNCs prepared are sufficiently stable over a one-month period to be useful. The most important advantage of reuse stability is the effective reduction of cost in industry applications. However, further studies on this are required.

Also, the APTES coating does not seem to have a very pronounced effect on catalase-like activity. Activity was confirmed to be higher at the optimum pH value of 7.4, and so was stability, as NPs are more stable due to the APTES molecules allowing a greater decomposition of hydrogen peroxide and C10A clays' hydrophobic properties, as already mentioned. This is in accordance with the literature. [54]

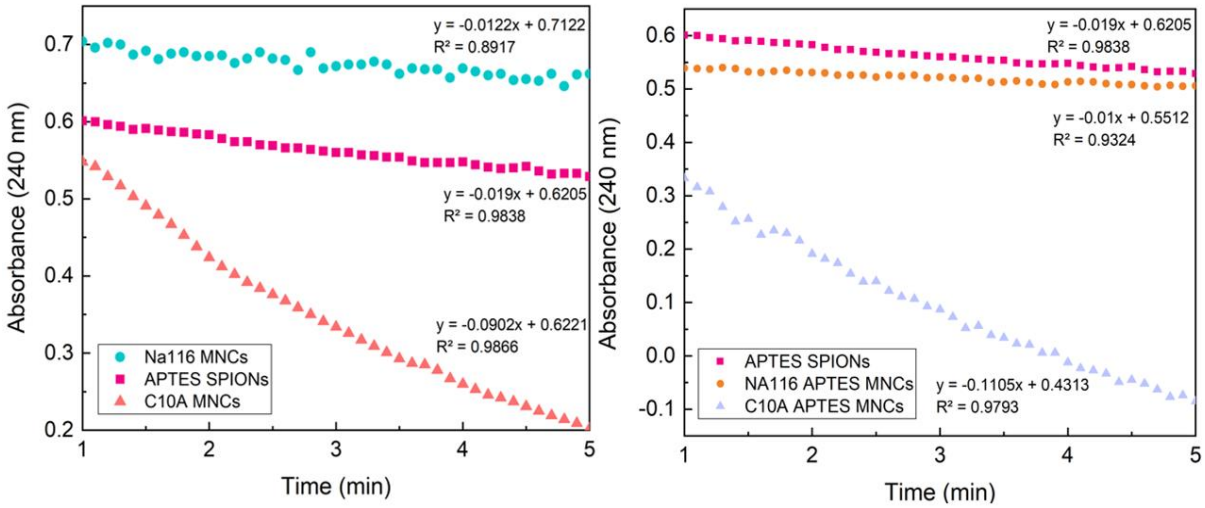

Figure 19 - **Effect of surface coatings on catalase-like activity of MNCs pH 6.** These assays were carried out using a specific quantity of 5 mg mL^{-1} APTES or MNCs, 20 µL of H_2O_2 0.88 M, in 1mL of phosphate buffer (10 mM, pH 6). The assays were made in duplicate.

Table 7 - **Specific activity values** of APTES coated SPIONs and all magnetic nanoclays for **catalase-like activity** at **pH 6.**

Specific activity (U mg^{-1})	**APTES SPIONs**	**NA116 MNCs**	**NA116 APTES MNCs**	**C10A MNCs**	**C10A APTES MNCs**
First assay	6.8 ± 0.4 (100%)	0.7 ± 0.2	1.2 ± 0.1	6.5 ± 0.7	5.3 ± 0.1
1 week after	5.6 ± 0.3 (82%)	0.55 ± 0.06 (74%)	0.75 ± 0.04 (64%)	6.5 ± 0.2 (100%)	5.3 ± 0.1 (100%)
1 month after	7.6	0.52 (70%)	0.70 (60%)	5.9 (90%)	4.4 (84%)

CONCLUSIONS AND FUTURE PERSPECTIVES

The main goal of this research work was to develop magnetic nanoclays with catalase and peroxidase-like activities for cancer treatment application.

SPIONs were used as they possess unique properties, such as their biocompatibility and their ability to generate heat when subjected to a magnetic field as well as due to their newly found peroxidase-like and catalase-like activity. They were produced using the chemical co-precipitation method. Due to their low stability in aqueous suspension, SPIONs were also coated with (3-aminopropyl) triethoxysilane, commonly known as APTES. The synthesized uncoated SPIONs and APTES SPIONs were encapsulated into different types of montmorillonite clays' interlaminar space (MMT and organic modified MMT) to evaluate how effective this strategy might be in association with their catalytic activity. Therefore, they were characterized by FTIR, XRD, SEM EDS and TGA.

Through FTIR, it was possible to observe the characteristic bands of functional groups of the coating, proving that the surface modification and encapsulation of magnetic nanoclays occurred. XRD analysis confirmed that the NPs coated with APTES maintained the crystalline structure of naked NPs. Also, it was concluded that there were not significative changes for all magnetic nanoclays in their d spacing, even though intercalation has been clearly achieved to some extent. Therefore, it is not possible to say there was a complete intercalation of MNCs, so an increased concentration of NPs would be necessary to achieve larger distances between the aluminosilicate layers. However, for Na116 MNCs the appearance of another peak, regarding NPs, confirmed the intercalation and increasing in d spacing. For Na116 APTES MNCs the changes in d spacing were not significant due to the quantity of APTES coating in the NPs being probably small.

SEM confirmed the morphology of each magnetic nanoclay having the desired properties such as MMT layered structure. For OMMT the changing in morphology was quite evident, showing a more disordered structure with flake-like aggregates. EDS showed the presence of elements such as oxygen, carbon, iron, nitrogen, silica, aluminium, sodium, magnesium, and calcium in the MMT and magnetic nanoclays surface. Also, the presence of peaks related to the binding energies of MMT, and the peaks related to Fe_3O_4 NPs, confirmed their intercalation in the clays. Concerning OMMT, most of the Na^+ cations on the MMT clay surface have been exchanged by the alkylammonium cations, demonstrating the potential of organophilization. On the side of C10A APTES MNCs, it was concluded that a partial intercalation may have occurred because APTES coating on NPs is almost not present, for some reason, due to its lower weight percentage of iron and almost inexistent nitrogen, given by the EDS results. Hence, it was observed that the synthesis of Na116 MNCs and Na116 APTES MNCs was more successful. SEM results indicate that NPs were intercalated in between the clays' interlaminar space, and it was confirmed by XRD analysis.

Finally, with DSC-TGA it was possible to obtain the quantity of NPs incorporated in each magnetic nanoclay and study its thermal stability. The Na116 clays in the presence of APTES NPs have less temperature variation compared to pristine MMT and it degrades more than Na116 MNCs, since Fe_3O_4 NPs do not degrade with temperature in the tested range, as proved.

Magnetic hyperthermia assays of magnetic nanoclays showed a higher temperature variation and SAR for Na116 MNCs, as expected. However, it was concluded that a 20% (w/w) of SPIONs with a concentration of 2.5 mg mL^{-1} is enough to achieve the desired temperature variations. Magnetic nanoclays within the tested conditions are able to reach the temperature difference of 5 ºC, indicating that they can reach 42 ºC which is the theoretical temperature of the tumor cells to enter the apoptotic phase.

Moreover, all these studies suggest that montmorillonite magnetic clays used here can act as an effective support for cancer treatment. Following NPs and MNCs characterization, it was important to assess their enzymatic-like activities. For peroxidase-like activity, the assays were carried out using TMB as a substrate. The pH of the activity was evaluated for sodium acetate buffer pH 3.5 (100 mM). However, to better mimic the intra-cellular environment of lysosomes and the cytosol it is necessary to study a closer pH to the physiological one. The results obtained suggested that the loss of activity was more evident when an APTES coating was present, and therefore, it does not have a stabilizing effect. A possible explanation for this is due to their positive charge that have a lower affinity towards the TMB. After a one-month storage, the C10A APTES MNCs almost completely loss their catalytic activity because of the oxidation of the NPs. Nevertheless, it was expectable that after a month the peroxidase-like activity would be reduced, but still, present. The results proved that all suspensions still possess some retained catalytic activity at an acidic pH, but Na116 MNCs combined the best stability with the highest specific peroxidase-like activity.

The catalase-like activity assays were assessed at 240 nm measuring the decomposition of hydrogen peroxide. For this assay, the activity was measured using phosphate buffer at pH 7.4 (10 mM). It was observed that the presence of an APTES coating has little effect on the catalase-like activity of MNCs freshly produced or over a week. After one-month storage, APTES coating seems to have a stabilizing effect, especially in C10A MNCs. In general, the values obtained after a week storage are lower than expected, since the tendency seems to be high stability of the NPs until one month of storage. This lower activity values might be the consequence of a systematic error caused using an incorrectly calibrated micropipette.

Concerning the catalase-like activity at pH 6, it was confirmed that it exists, and the presence of an APTES coating improves the catalase-like activity of Na116 MNCs. In contrast, it was verified that for C10A MNCs the catalytic activity is restrained. This was already evident at pH 7.4, but less noticeable. The catalytic activity was seen to be hampered by the hydrophobic properties of the organic modifier, lowering the catalase-like activity of C10A APTES MNCs compared to C10A MNCs. Over a period of one month, all NPs except APTES SPIONS showed a decrease in specific catalase-like activity. This loss of activity may be a consequence of NPs oxidation.

The errors associated to the catalytic activity values measured were high, so the MNCs suspensions must be well shaken before pipetting the amounts needed amount for and more replicas should have been done. In conclusion, all magnetic clays still exhibit peroxidase-like activity and catalase-like activity, being at least granted one month of stability in an aqueous suspension. Also, it was concluded that APTES coating does not seem to have a very pronounced effect on catalase-like activity for both pH. Therefore, the catalytic activity was confirmed to be higher at the optimum pH value of 7.4, and so was stability. The overall results in this work showed the potential of these magnetic nanoclays' with catalytic activity for cancer treatment application. However, it is still necessary to go forward with cytotoxicity tests.

To assess the therapy's effectiveness, future work should be done to mimic when SPIONs are injected in the body or directly into the tissue, tumor cells take up the SPIONs and stay fixed. These assays should then be compared to *in vitro* magnetic hyperthermia to better assess the effects of the inexistent Brownian relaxation. Also, following magnetic hyperthermia, cell viability and cytotoxicity tests (including hydrogen peroxide concentration dependence) should be performed to detect levels of cell apoptosis. Hydrogen peroxide is one of the main components of catalase-like activity, however, it is a highly toxic one and the amounts formerly used would be severely cytotoxic for cells. Some additional tests should be done to see if the concentration could be lowered.

The research done in this dissertation is just the beginning of all the work needed to use this as a solution to cancer treatment. The study on the applicability of the MNCs produced is necessary. Thus,

it would be of great interest to evaluate all these parameters for other iron concentrations which certainly will influence the catalytic activity of magnetic nanoclays and the pH dependence. Another aspect being considered is using another surface coating, for example DMSA, as it was not possible to use this coating for the purpose due to problems with the equipment to proceed the DMSA NPs' synthesis. However, the procedure with APTES coating had no limitations and was evaluated. As in this work only therapeutic features were considered, it would be valuable to study more in depth the diagnosis features of MNCs for MRI purposes, so that the theranostics system would be more fully assessed.

REFERENCES

[1] "New cases of cancer 2020". https://gco.iarc.fr/today/home (accessed June 2022)

[2] L. Chen, C. Hui, S. Fiore, D. Shen, H. Zhang, and C. Sheng, "Applied Clay Science Functional magnetic nanoparticle/clay mineral nanocomposites : preparation, magnetism and versatile applications", *Appl. Clay Sci.*, vol. 127–128, pp. 143–163, 2016, doi: 10.1016/j.clay.2016.04.009.

[3] R. A. Bini, R. Fernando, C. Marques, F. J. Santos, J. A. Chaker, and M. Jafelicci, "Synthesis and functionalization of magnetite nanoparticles with different amino-functional alkoxysilanes," *J. Magn. Magn. Mater.*, vol. 324, no. 4, pp. 534–539, 2012, doi:10.1016/j.jmmm.2011.08.035.

[4] A. Kumar and M. Gupta, "Synthesis and surface engineering of iron oxide nanoparticles for biomedical applications", *Biomaterials*, vol. 26, no. 18, pp. 3995–4021, 2005, doi: 10.1016/j.biomaterials.2004.10.012.

[5] P. I. P. Soares *et al.*, "Effects of surfactants on the magnetic properties of iron oxide colloids," *J. Colloid Interface Sci.*, vol. 419, pp. 46–51, Apr. 2014, doi: 10.1016/j.jcis.2013.12.045.

[6] I. W. Hamley, "Nanotechnology with Soft Materials," *Angewandte Chemie International Edition*, vol 42, no. 15, pp. 1692–1712, 2003, doi: 10.1002/anie.200200546.

[7] S. H. Doak, "Potential toxicity of superparamagnetic iron oxide nanoparticles (SPION)", *Nano Reviews*, vol. 1, pp. 1–15, 2010, doi: 10.3402%2Fnano.v1i0.5358.

[8] A. I. Journal, R. Vakili-ghartavol, A. A. Momtazi-borojeni, and Z. Vakili-, "Toxicity assessment of superparamagnetic iron oxide nanoparticles in different tissues," *Artif. Cells, Nanomedicine, Biotechnol.*, vol. 48, no. 1, pp. 443–451, 2020, doi: 10.1080/21691401.2019.1709855.

[9] P. Morales and L. Ban, "Magnetic nanoparticles coated with dimercaptosuccinic acid: development, characterization, and application in biomedicine," *Journal of Nanoparticle Research*, 2014, doi: 10.1007/s11051-014-2589-6.

[10] M. Talelli *et al.*, "Superparamagnetic Iron Oxide Nanoparticles Encapsulated in Biodegradable Thermosensitive Polymeric Micelles: Toward a Targeted Nanomedicine Suitable for Image-Guided Drug Delivery," *Langmuir*, vol. 25, no. 4, pp. 2060–2067, 2009, doi: 10.1021/la8036499

[11] "Chelating agent". https://www.corrosionpedia.com/definition/254/chelating-agent (accessed June 2022)

[12] O. R. Sohani, A. A. Phatak, and P. D. Chaudhari, "Use of Nanocomposites in Drug Delivery Systems" *Pharma Times*, vol. 47, no. 4, pp 33-35, 2015.

[13] S. L. Bee, M. A. A. Abdullah, S. T. Bee, L. T. Sin, and A. R. Rahmat, "Polymer nanocomposites based on silylated-montmorillonite: A review," *Prog. Polym. Sci.*, vol. 85, pp. 57–82, 2018, doi: 10.1016/j.progpolymsci.2018.07.003.

[14] A. Abdul, K. Yop, S. Jin, and D. Hui, "Epoxy clay nanocomposites – processing, properties and applications: A review," *Compos. Part B*, vol. 45, no. 1, pp. 308–320, 2013, doi: 10.1016/j.compositesb.2012.04.012.

[15] S. Pavlidou and C. D. Papaspyrides, "A review on polymer – layered silicate nanocomposites," *Progress in Polymer Science*, vol. 33, no 12, pp. 1119–1198, 2008, doi: 10.1016/j.progpolymsci.2008.07.008

[16] S. Leporatti and R. Fakhrullin, "Recent advances in the design of inorganic and nano-clay particles for the treatment of brain disorders," *Journal of Materials Chemistry B*, vol. 9, no. 12, pp. 2756-2784, 2021, doi: 10.1039/D0TB02957B.

[17] L. Gao, J. Zhuang, L. Nie, *et al.*, "Intrinsic peroxidase-like activity of ferromagnetic nanoparticles", *Nature Nanotechnology*, vol. 2, no. 9, pp. 577–583, Aug. 2007, doi: 10.1038/nnano.2007.260.

[18] B. Jiang, D. Duan, L. Gao, *et al.*, "Standardized assays for determining the catalytic activity and kinetics of peroxidase-like nanozymes", *Nature Protocols*, vol. 13, no. 7, pp. 1506–1520, Jul. 2018, doi: 10.1038/s41596-018-0001-1.

[19] M. B. Nita and A. Grzybowski, "The Role of the Reactive Oxygen Species and Oxidative Stress in the Pathomechanism of the Age-Related Ocular Diseases and Other Pathologies of the Anterior and Posterior Eye Segments in Adults," *Oxid Med Cell Longev*, vol. 2016, pp. 1-23, 2016, doi: 10.1155/2016/3164734.

[20] M. Li, H. Zhang, Y. Hou, *et al.*, "State-of-the-art iron-based nanozymes for biocatalytic tumor therapy", *Nanoscale Horizons*, vol. 5, no. 2, pp. 202–217, 2020, doi: 10.1039/C9NH00577C.

[21] P. D. Josephy, T. Eling, and R. P. Mason, "The horseradish peroxidase-catalyzed oxidation of 3,5,3',5' tetramethylbenzidine: free radical and charge-transfer complex intermediates.", *Journal of Biological Chemistry*, vol. 257, no. 7, pp. 3669–3675, Apr. 1982, doi: 10.1016/s0021-9258(18)34832-4.

[22] Z. Chen, J.-J. Yin, Y.-T. Zhou, *et al.*, "Dual enzyme-like activities of iron oxide nanoparticles and their implication for diminishing cytotoxicity", *ACS Nano*, vol. 6, no. 5, pp. 4001–4012, May 2012, doi: 10.1021/nn300291r.

[23] W. He, W. Wamer, Q. Xia, J.-j. Yin, and P. P. Fu, "Enzyme-like activity of nanomaterials", *Journal of Environmental Science and Health, Part C*, vol. 32, no. 2, pp. 186–211, Apr. 2014, doi: 10.1080/10590501.2014.907462.

[24] J. Wu, X. Wang, Q. Wang, *et al.*, "Nanomaterials with enzyme-like characteristics (nanozymes): Next-generation artificial enzymes (II)", *Chemical Society Reviews*, vol. 48, no. 4, pp. 1004–1076, 2019, doi: 10.1039/c3cs35486e.

[25] Jordan, A. Wust P. et al. "Cellular uptake of magnetic fluid particles and their effects on human adenocarcinoma cells exposed to AC magnetic fields in vitro." *International journal of hyperthermia*, vol. 12 no. 6, pp.705–22, 1996, doi: 10.3109/02656739609027678.

[26] M. R. Horsman and J. Overgaard, "Hyperthermia: a Potent Enhancer of Radiotherapy," *Clin Oncol (R Coll Radiol)*, vol. 19, no 6. pp. 418–426, 2007, doi: 10.1016/j.clon.2007.03.015.

[27] C. S. S. R. Kumar and F. Mohammad, "Magnetic nanomaterials for hyperthermia-based therapy and controlled drug delivery," *Adv. Drug Deliv. Rev.*, vol. 63, no. 9, pp. 789–808, 2011, doi: 1016/j.addr.2011.03.008.

[28] G. Hemery, O. Sandre, D. Ortega, E. Garaio, and F. Plazaola, "Fundamentals and advances in magnetic hyperthermia," vol. 41302, 2015, doi: 10.48550/arXiv.1510.06383.

[29] P. I. P. Soares *et al.*, "Iron oxide nanoparticles stabilized with a bilayer of oleic acid for magnetic hyperthermia and MRI applications," *Appl Surf Sci*, vol. 383, pp. 240–247, Oct. 2016, doi: 10.1016/j.apsusc.2016.04.181.

[30] Chou, Chung-Kwang. "Use of heating rate and specific absorption rate in the hyperthermia clinic." *International Journal of Hyperthermia*, vol 6 no. 2, pp. 367–370, 1990, doi: 10.3109/02656739009141144.

[31] B. Kozissnik, A. C. Bohorquez, J. Dobson, and C. Rinaldi, "Magnetic fluid hyperthermia: Advances, challenges, and opportunity," *International Journal of Hyperthermia*, vol. 29, no. 8. Informa Healthcare, pp. 706–714, 2013, doi: 10.3109/02656736.2013.837200.

[32] M. H. Mashhadizadeh and M. Amoli-diva, "Drug-Carrying Amino Silane Coated Magnetic Nanoparticles as Potential Vehicles for Delivery of Antibiotics". *Journal of Nanomedicine & Nanotechnology*, vol. 3, no. 4, pp. 3–9, 2012, doi: 10.4172/2157-7439.1000139.

[33] M. Validi, Q. Branch, S. Bazgir, A. Rashidi, and M. E. Yazdanshenas. "Intercalation of methylene blue into montmorillonite at different conditions: An approach for preparing clay-based nanopigments". *Ceramics Silikaty.* vol. 56. no. 2, pp. 152-158, 2012.

[34] Mascolo, M.C.; Pei, Y.; Ring, T.A. "Room Temperature Co-Precipitation Synthesis of Magnetite Nanoparticles in a Large pH Window with Different Bases." *Materials*, vol. *6*, no. 12, pp. 5549-5567. 2013, doi: 10.3390/ma6125549.

[35] P. I. P. Soares *et al.*, "Thermal and magnetic properties of iron oxide colloids: influence of surfactants," *Nanotechnology*, vol. 26, no. 42, Oct. 2015, doi: 10.1088/0957-4484/26/42/425704.

[36] Peng Yuan, Peter D. Southon, Zongwen Liu, Malcolm E. R. Green, James M. Hook, Sarah J. Antill, and Cameron J. Kepert. "Functionalization of Halloysite Clay Nanotubes by Grafting with γ-Aminopropyltriethoxysilane." *The Journal of Physical Chemistry C*, vol. 112, no. 40, 2008, doi: 10.1021/jp805657t.

[37] Bo Zhang, et al. "Hydrothermal Synthesis of a graphene/magnetite/montmorillonite nanocomposite and its ultrasonically assisted methylene blue adsorption." *Journal of materials science*, vol. 54, no.16, pp. 11037-11055, 2019, doi: 10.1007/s10853-019-03659-6.

[38] S. Yelkovan, D. Yılmaz, and K. Aksoy, "A study of organo-modified clay type on pet-clay based nanocomposite properties," *Usak University Journal of Material Sciences*, vol. 1, pp. 33–46, 2014, doi: 10.12748/uujms.201416498.

[39] G. Gnanaprakash, S. Mahadevan, T. Jayakumar, P. Kalyanasundaram, J. Philip, and B. Raj, "Effect of initial pH and temperature of iron salt solutions on formation of magnetite nanoparticles," *Journal of Materials and Chemistry*, vol. 103, pp. 168–175, 2007, doi: 10.1016/J.MATCHEMPHYS.2007.02.011.

[40] Y. Li, H. Chen, J. Wu, Q. He, Y. Li, W. Yang, Y. Zhou, "Preparation and characterization of APTES modified magnetic MMT capable of using anisotropic nanoparticles", *Applied Surface Science*, vol. 447, pp. 393-400, 2018, doi: 10.1016/j.apsusc.2018.03.230

[41] K. Kalantari *et al.*, "Size-Controlled Synthesis of Fe_3O_4 Magnetic Nanoparticles in the Layers of Montmorillonite," *Journal of Nanomaterials*, vol 1-9. 2014, doi: 10.1155/2014/739485.

[42] Villa S, Riani P, Locardi F, Canepa F., "Functionalization of Fe_3O_4 NPs by Silanization: Use of Amine (APTES) and Thiol (MPTMS) Silanes and Their Physical Characterization". *Materials (Basel)*, vol. 9, no. 10, Oct. 2016, doi: 10.3390/ma9100826.

[43] M. G. Martins *et al.*, "Synthesis and characterization of montmorillonite clay intercalated with molecular magnetic compounds," *J. Solid State Chem.*, vol. 228, pp. 99–104, 2015. doi: 10.1016/j.jssc.2015.04.024

[44] X. Zheng, J. Dou, J. Yuan, W. Qin, X. Hong, and A. Ding, "Removal of Cs^+ from water and soil by ammonium-pillared montmorillonite/Fe_3O^4 composite," *JES*, pp. 1–13, 2016, doi: 10.1016/j.jes.2016.08.019.

[45] G. Kandasamy and D. Maity, "Recent advances in superparamagnetic iron oxide nanoparticles (SPIONs) for in vitro and in vivo cancer nanotheranostics," *Int. J. Pharm.*, vol. 496, no. 2, pp. 191–218, 2015. doi: 10.1016/j.ijpharm.2015.10.058.

[46] S. Pernal, V. M. Wu, and V. Uskoković, "Hydroxyapatite as a Vehicle for the Selective Effect of Superparamagnetic Iron Oxide Nanoparticles against Human Glioblastoma Cells," *ACS Appl. Mater. Interfaces*, vol. 9, no. 45, pp. 39283–39302, 2017. doi: 10.1021/acsami.7b15116.

[47] K. D. Bakoglidis, K. Simeonidis, D. Sakellari, G. Stefanou and M. Angelakeris, "Size-Dependent Mechanisms in AC Magnetic Hyperthermia Response of Iron-Oxide Nanoparticles," *in IEEE Transactions on Magnetics*, vol. 48, no. 4, pp. 1320-1323, April 2012, doi: 10.1109/TMAG.2011.2173474.

[48] Adolph L., Lorenz R.: "Enzyme Diagnosis in Diseases of the Heart, Liver and Pancreas". *Basel, Karger*, pp 29-50, 1982, doi:10.1159/000403334.

[49] B. Jiang, D. Duan, L. Gao, *et al.*, "Standardized assays for determining the catalytic activity and kinetics of peroxidase-like nanozymes", *Nature Protocols*, vol. 13, no. 7, pp. 1506–1520, Jul. 2018, doi: 10.1038/s41596-018-0001-1.

[50] Y. Huang, J. Ren, and X. Qu, "Nanozymes: Classification, catalytic mechanisms, activity regulation, and applications", *Chemical Reviews*, vol. 119, no. 6, pp. 4357–4412, doi: 10.1021/acs.chemrev.8b00672.

[51] F. Yu, Y. Huang, A. J. Cole, and V. C. Yang, "The artificial peroxidase activity of magnetic iron oxide nanoparticles and its application to glucose detection", *Biomaterials*, vol. 30, no. 27, pp. 4716–4722, Sep. 2009, doi: 10.1016/j.biomaterials.2009.05.005.

[52] E. Johnson, P. Ostrowski, V. Jaumouillé, and S. Grinstein, "The position of lysosomes within the cell determines their luminal pH," *J. Cell Biol.*, vol. 212, no. 6, pp. 677–692, 2016, doi: 10.1083/jcb.201507112.

[53] "Absorbance reading on my spectrometer unstable or nonlinear at values above 1.0" https://www.vernier.com/til/2589 (accessed November 2022).

[54] L. Gao, K. Fan, and X. Yan, "Iron oxide nanozyme: A multifunctional enzyme mimetic for biomedical applications", *Theranostics*, vol. 7, no. 13, pp. 3207–3227, 2017. doi: 10.7150/thno.19738.

[55] J. Mu, L. Zhang, M. Zhao, and Y. Wang, "Catalase mimic property of Co_3o_4 nanomaterials with different morphology and its application as a calcium sensor", *ACS Applied Materials & Interfaces*, vol. 6, no. 10, pp. 7090–7098, May 2014. doi:10.1021/am406033q.

[56] Mahmoudi, M., Sant, S., Wang, B., Laurent, S. and Sen, T. "Superparamagnetic Iron Oxide Nanoparticles (SPIONs): Development, Surface Modification and Applications in

Chemotherapy." *Advanced Drug Delivery Reviews*, vol. 63, pp. 24-46, 2011, doi: 10.1016/j.addr.2010.05.006.

[57] Cervantes-Uc, J.M., Cauich-Rodríguez, J.V., Vázquez-Torres, H.; Garfias-Mesías, L.F., Paul, D.R. "Thermal degradation of commercially available organoclays studied by TGA–FTIR." *Thermochimica Acta*, vol. 457, pp. 92–102. 2007, doi: 10.1016/j.tca.2007.03.008.

[58] C. I. P. Chaparro, L. R. Loureiro, M. A. Valente, P. A. Videira, J. P. Borges, and P. I. P. Soares, "Application of hyperthermia for cancer treatment: Synthesis and characterization of magnetic nanoparticles and their internalization on tumor cell lines", *IEEE 6th Portuguese Meeting on Bioengineering*, 2019, doi: 10.1109/enbeng.2019.8692485.

[59] Cui, Hui-Wang & Fang, Qun & Du, Guan. "Structure of Intercalated Organic Montmorillonite and Its Pyrolysis Properties Analyzed Using Agrawal Integral Equation." *Science and Engineering of Composite Materials*, Dec. 2014. doi: 10.1515/secm-2012-0180.

[60] Y. J. Phua, W. S. Chow, and Z. A. M. Ishak, "Organomodification of Montmorillonite and its effects on the properties of poly (butylene succinate) nanocomposites," *Polymer Engineering & Science*, 2013, doi: 10.1002/pen.23460.

APPENDIX

A.1. Synthesis of SPIONs by chemical co-precipitation protocol

Adapted from Chaparro, 2017

Materials:

• $FeCl_3.6H_2O$: 5 mmol (1.35 g)
• $FeCl_2.4H_2O$: 2.5 mmol (0.49 g)
• NH_4OH 25%: 10 mL
• MilliQ water

Method:

1. Dissolve the ferrous and ferric chlorides into the milliQ water (2.5 mL for $FeCl_2.4H_2O$ and 10 mL for $FeCl_3.6H_2O$) and then add to the mixture another 50 mL milliQ water.
2. Deaeration of O_2 of the previous solutions with bubbling N_2.
3. Rapidly add 10 mL of ammonia solution under vigorous mechanical stirring (600 rpm) and kept for 5 minutes (color change from orange to black).
4. Stop the reaction by adding 60 mL milliQ water to the black solution formed.

A.1.1. Iron content determination by using the 1,10-phenanthroline calorimetric method.

Materials:

• Hydrochloric acid 37% (v/v)
• Hydroxylamine hydrochloride solution 100 mg mL^{-1}
• 500 µL of phenanthroline solution 3 mg mL^{-1}
• Ammonium acetate buffer (500 mM) pH 4
• HCl 0.01 M

Methods:

1. Dilute the sample to obtain a concentration in the range of 10 to 1000 $\mu g.mL^{-1}$ (brownish color).
2. Place 40 µL of diluted sample into an Eppendorf, followed by the addition of 20 µL of hydrochloric acid 37% (v/v).
3. Incubate the mixture for 1 hour at room temperature.
4. Add 100 µL of hydroxylamine hydrochloride solution, followed by 500 µL of phenanthroline solution.
5. Dilute the sample to 1800 µL with ammonium acetate buffer. (orange color)
6. Measure the absorbance of the samples at 510 nm using a UV-VIS spectrophotometer.
7. Determine the iron (II) concentration using the calibration curve.
8. To obtain the nanoparticles concentration use the formula [Fe] = 0.7 × [NPs].

A.2. SEM/EDS and EDX results

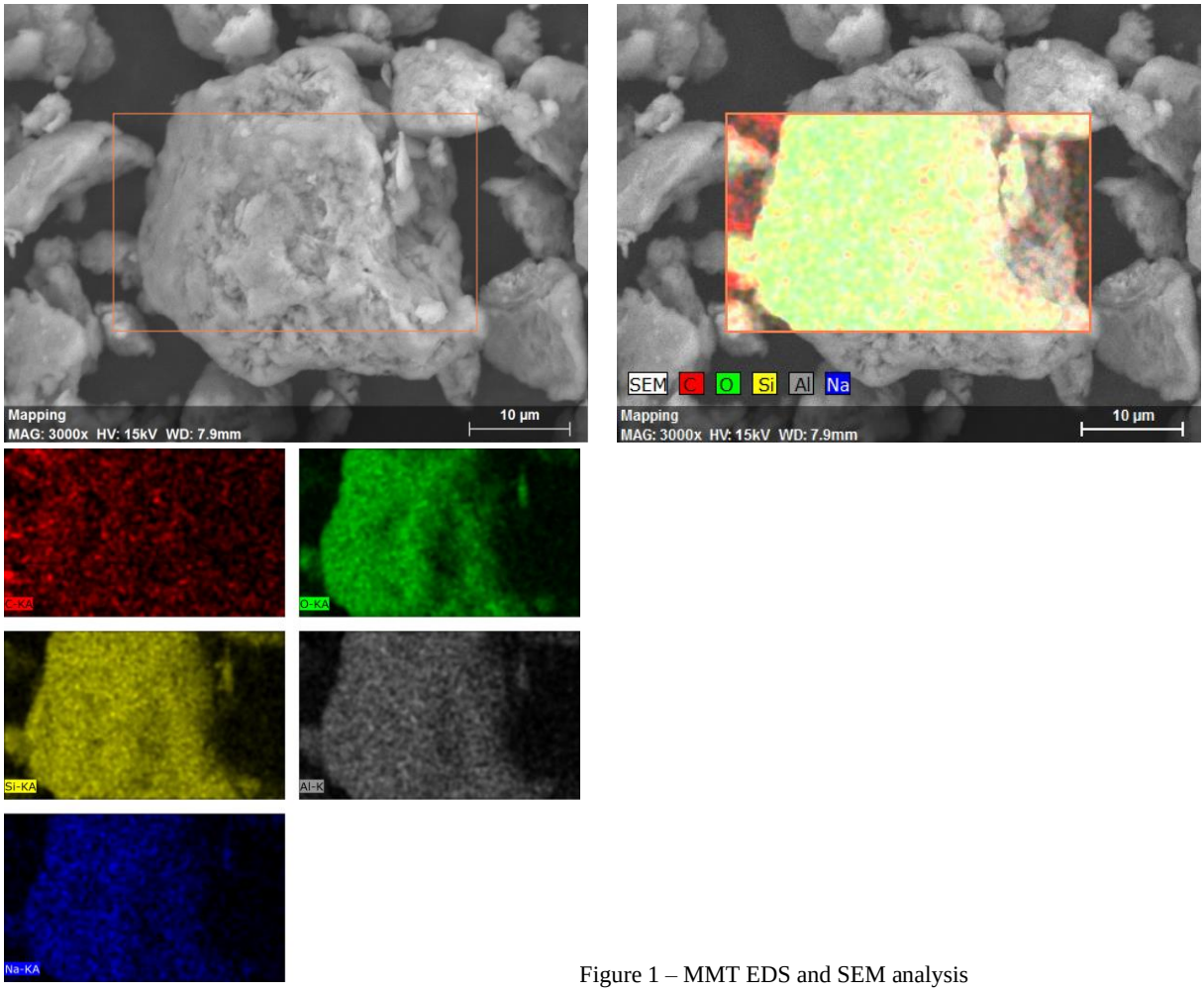

Figure 1 – MMT EDS and SEM analysis

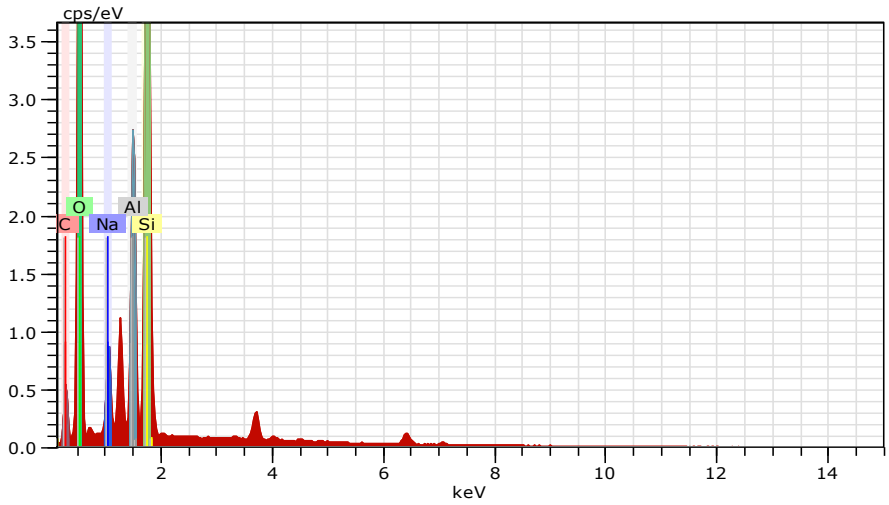

Figure 2 - **Energy dispersive X-ray spectroscopy** spectrum of **MMT** clay.

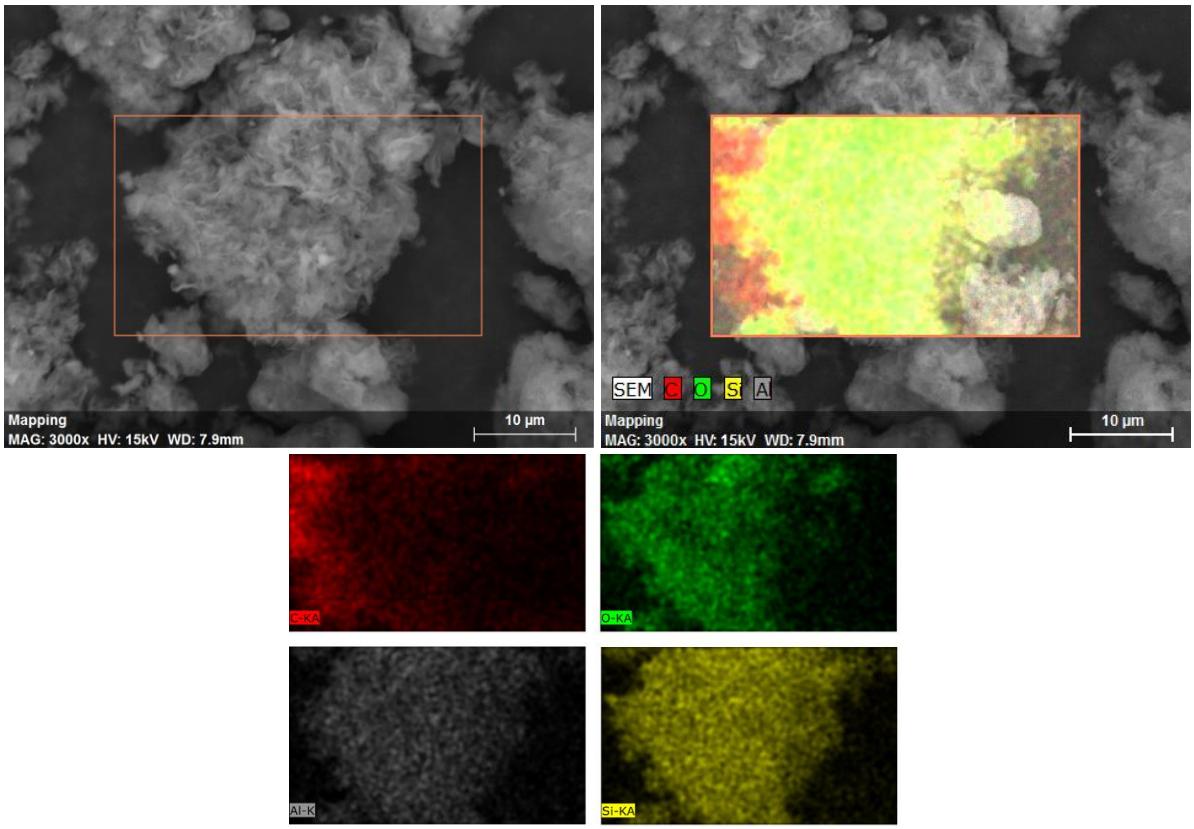

Figure 3 – OMMT EDS and SEM analysis

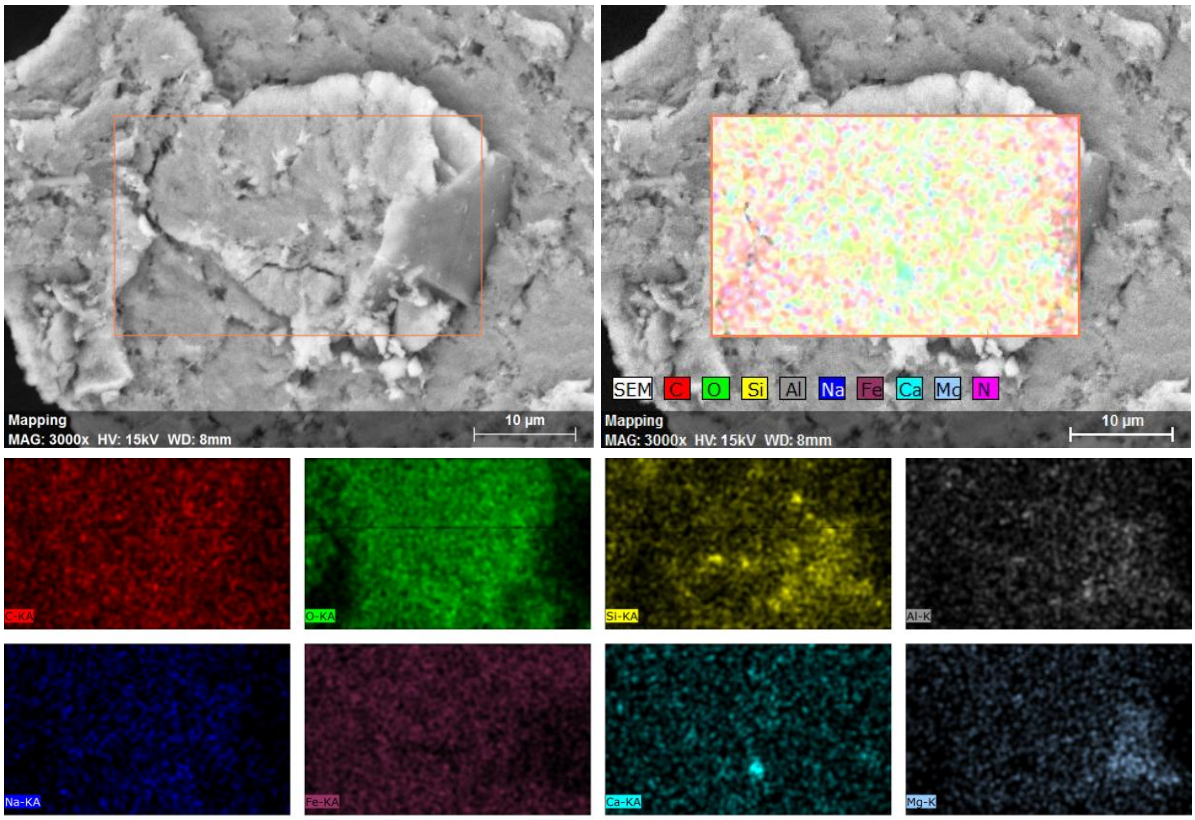

Figure 4 – Na116 MNCs EDS and SEM analysis

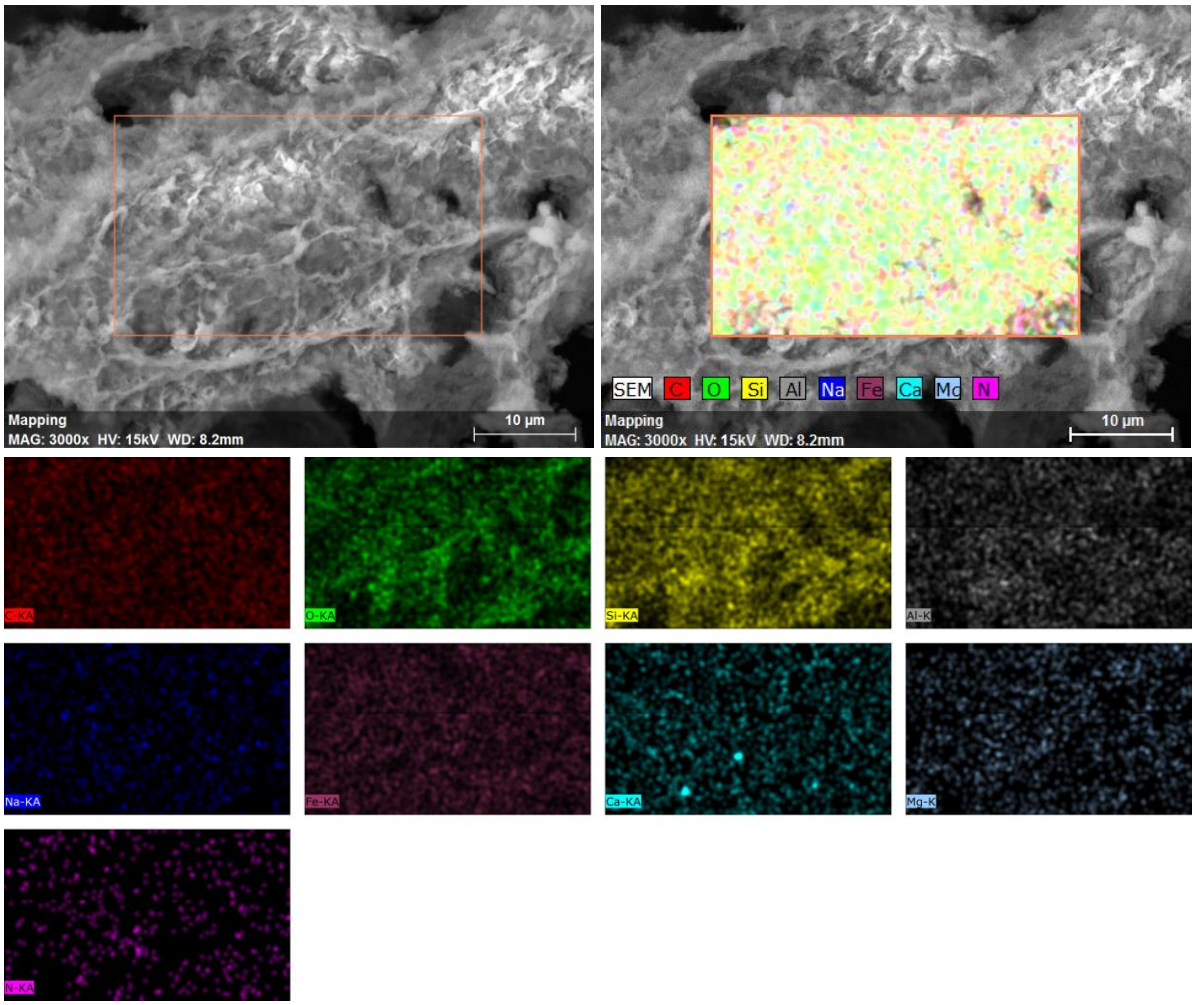

Figure 5 – Na116 APTES MNCs EDS and SEM analysis

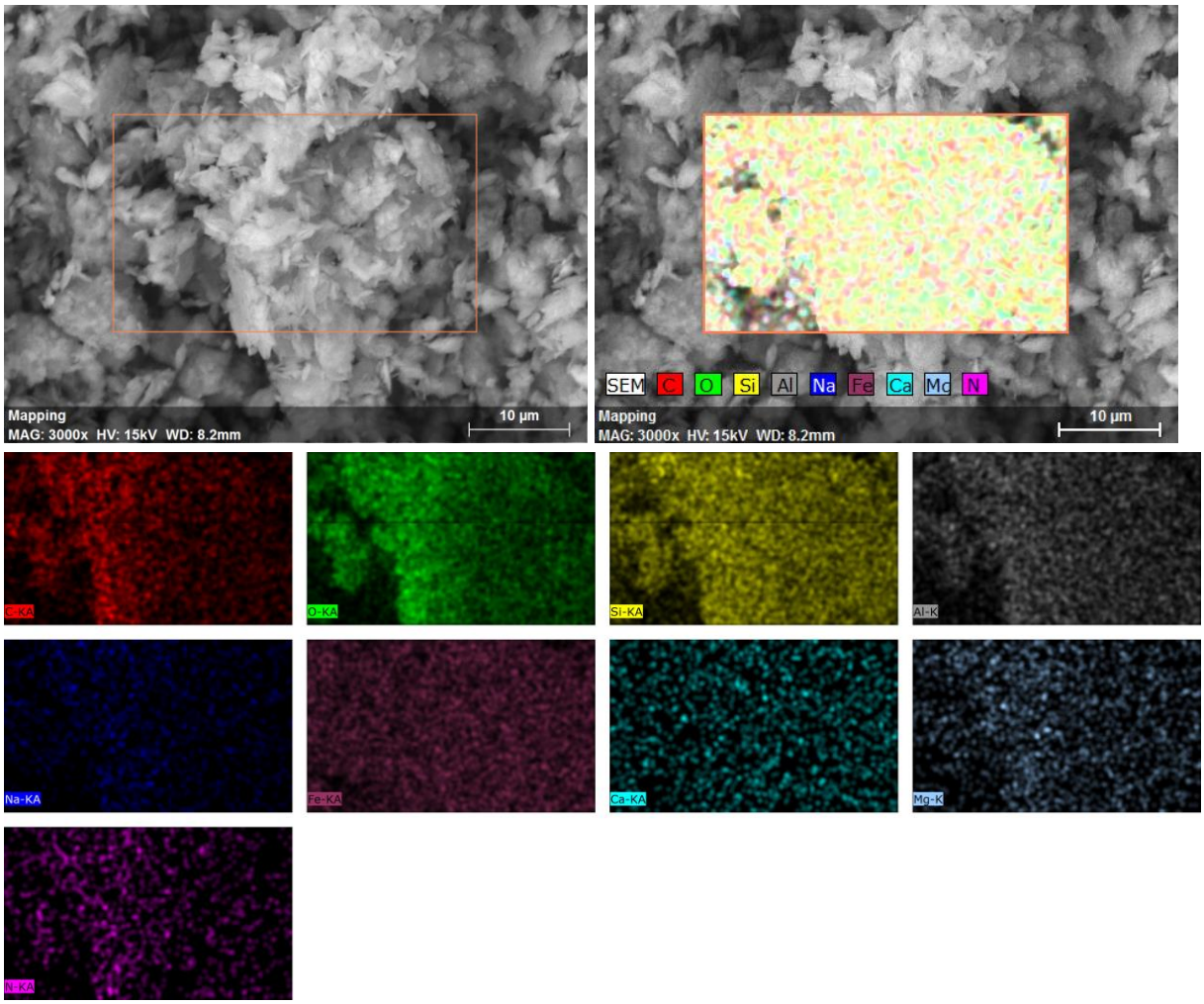

Figure 6 – C10A MNCs EDS and SEM analysis

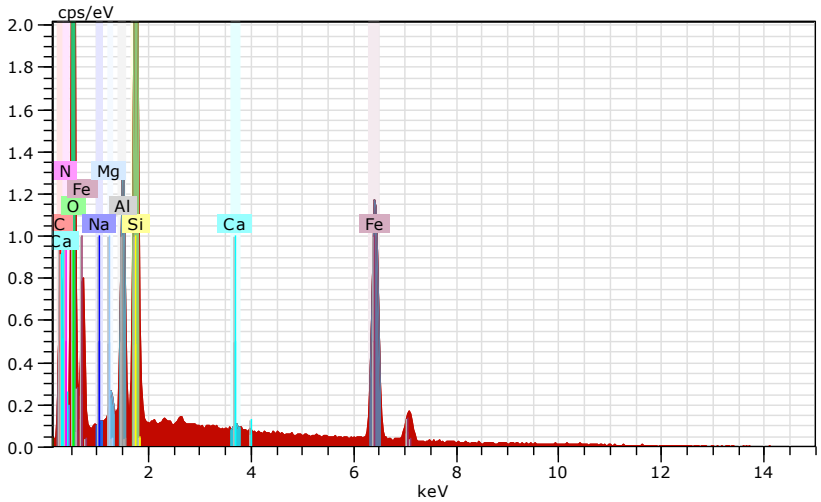

Figure 7 – C10A MNCs EDX analysis

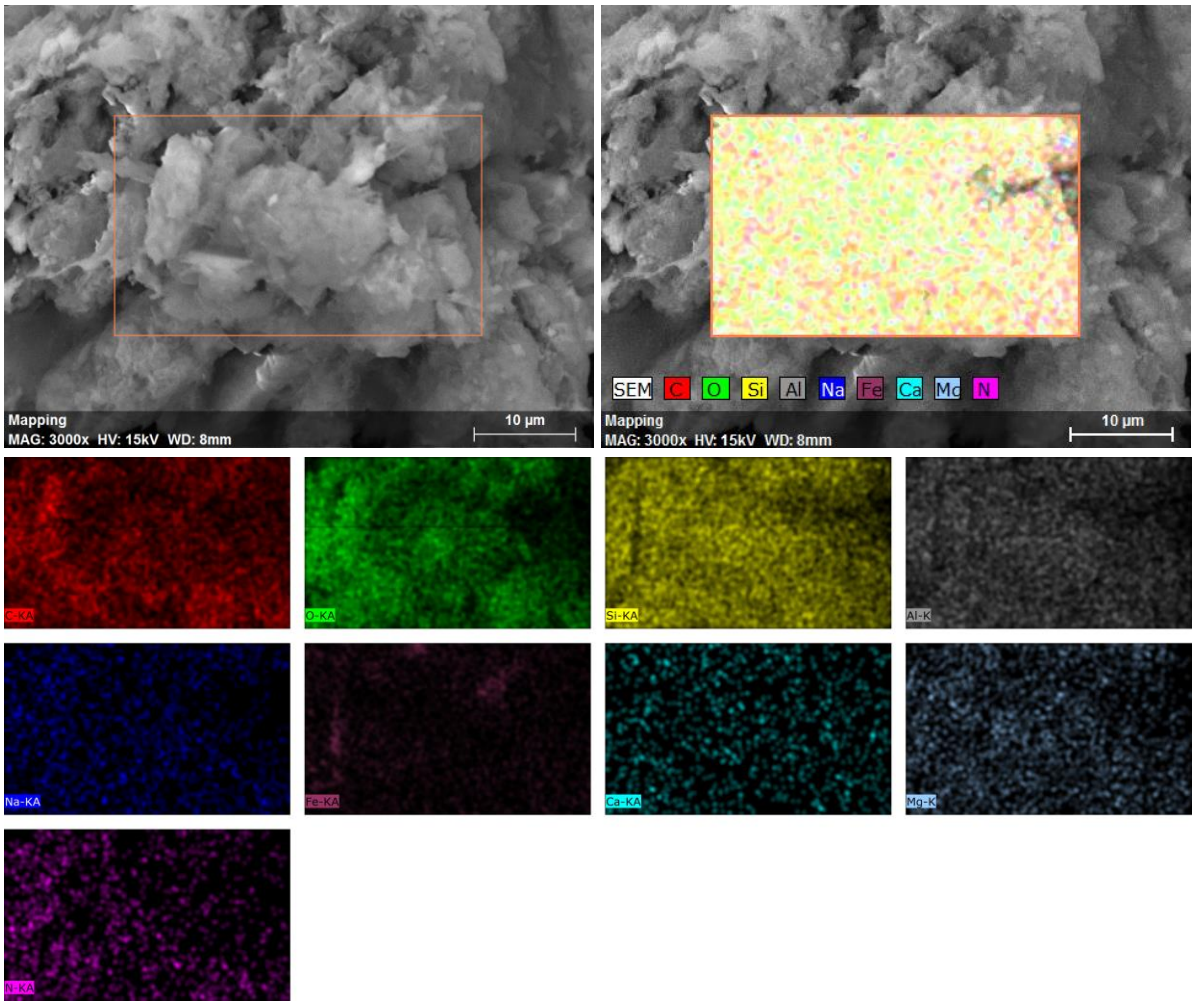

Figure 8 – C10A APTES MNCs EDS and SEM analysis

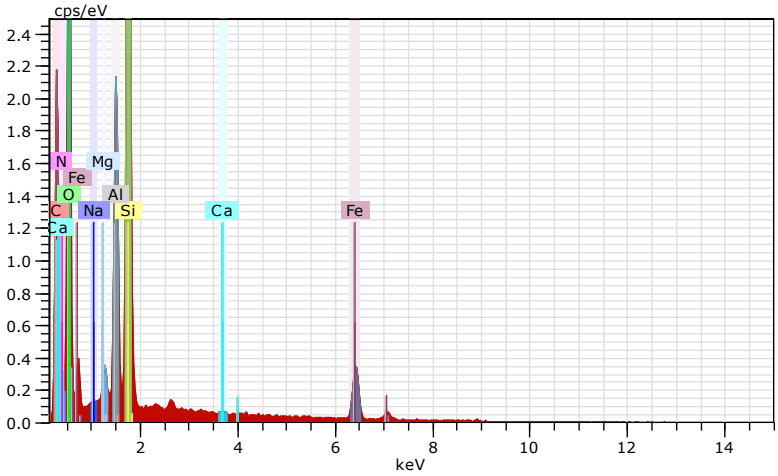

Figure 9 – C10A APTES MNCs EDX analysis